ESI for:

Coordination capabilities of bis-(2-pyridyl)amides in the field of divalent germanium, tin and lead compounds.

Jan Zechovský, Ondřej Mrózek, Maksim Samsonov, Roman Jambor, Aleš Růžička and Libor Dostál*

*E-mail: libor.dostal@upce.cz (L.D.)

Table of contents:

1) NMR spectra of studied compounds.

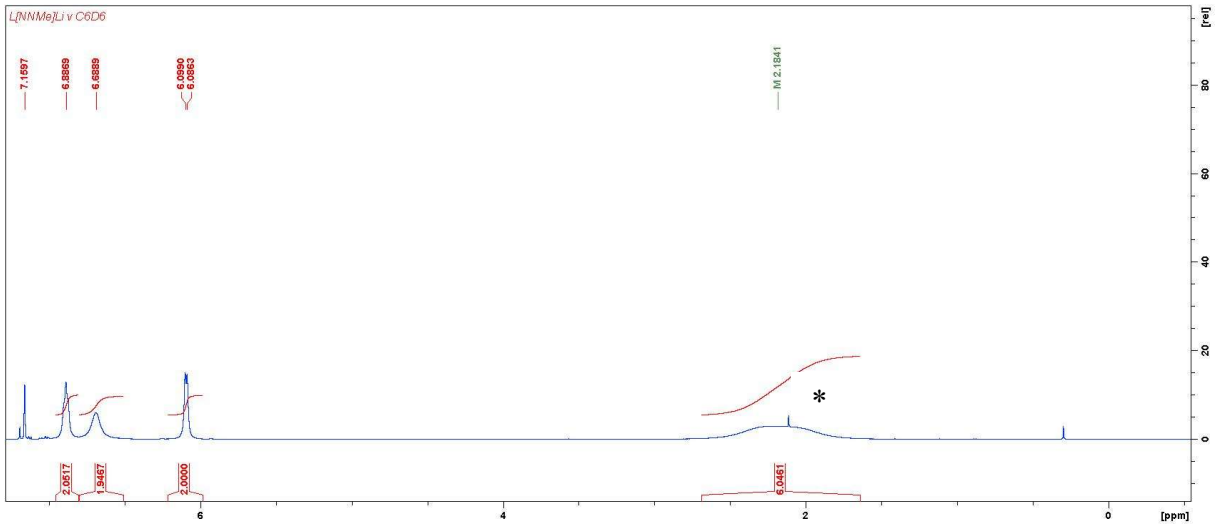

Figure S1: ^{1}H NMR spectrum of **2** in C_6D_6 (* traces of toluene).

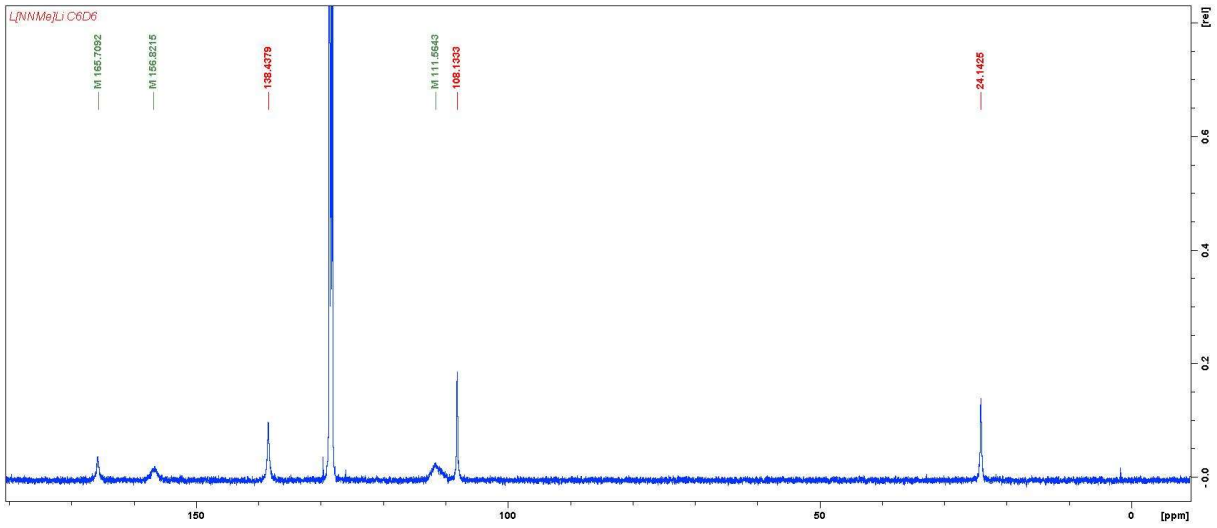

Figure S2: $^{13}C\{^{1}H\}$ NMR spectrum of **2** in C_6D_6.

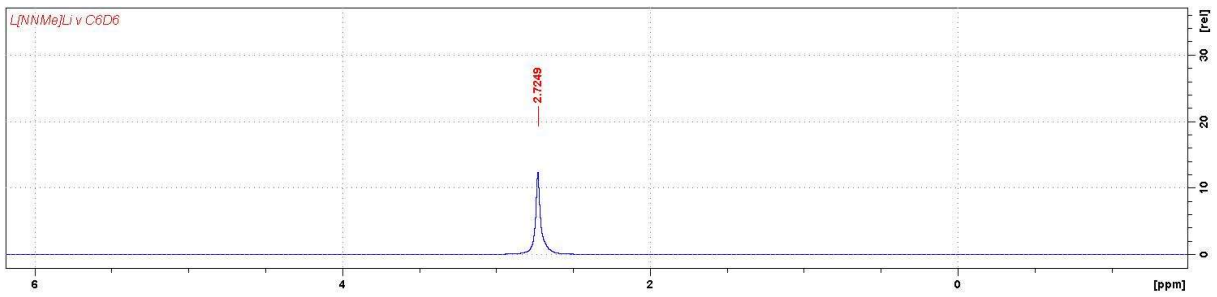

Figure S3: $^{7}Li\{^{1}H\}$ NMR spectrum of **2** in C_6D_6.

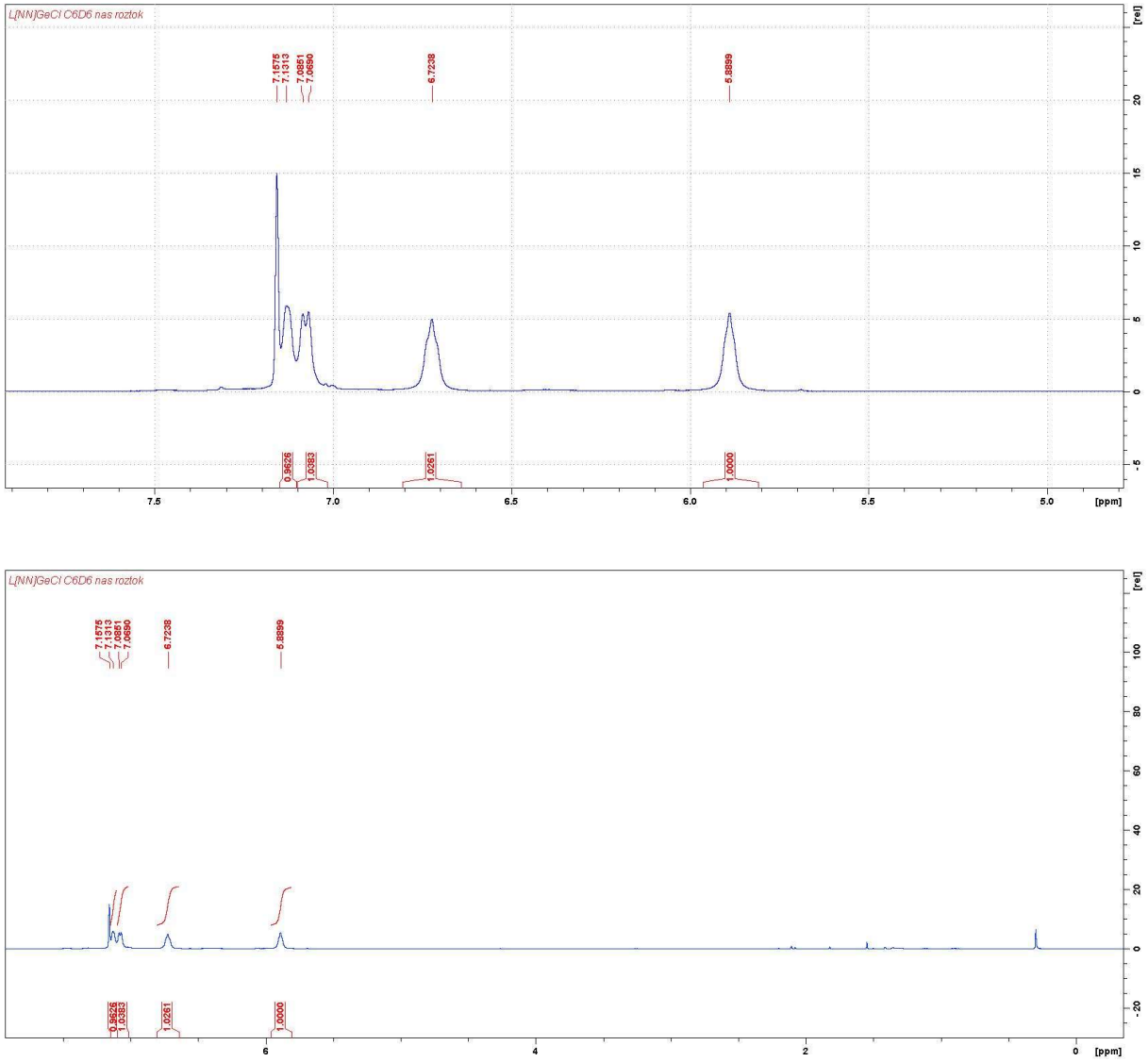

Figure S4: ^{1}H NMR spectrum of **3** in C_6D_6.

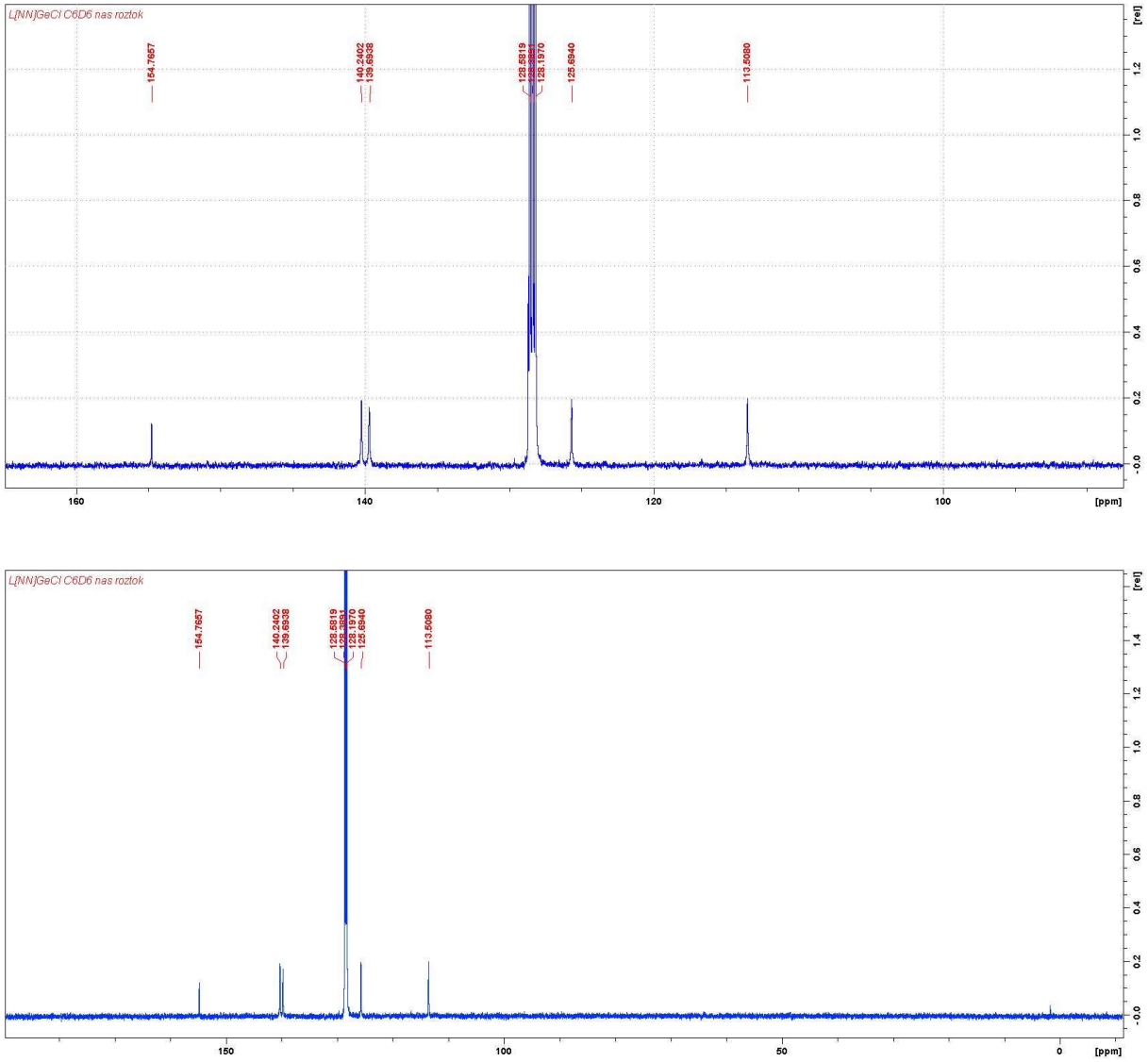

Figure S5: $^{13}C\{^{1}H\}$ NMR spectrum of **3** in C_6D_6.

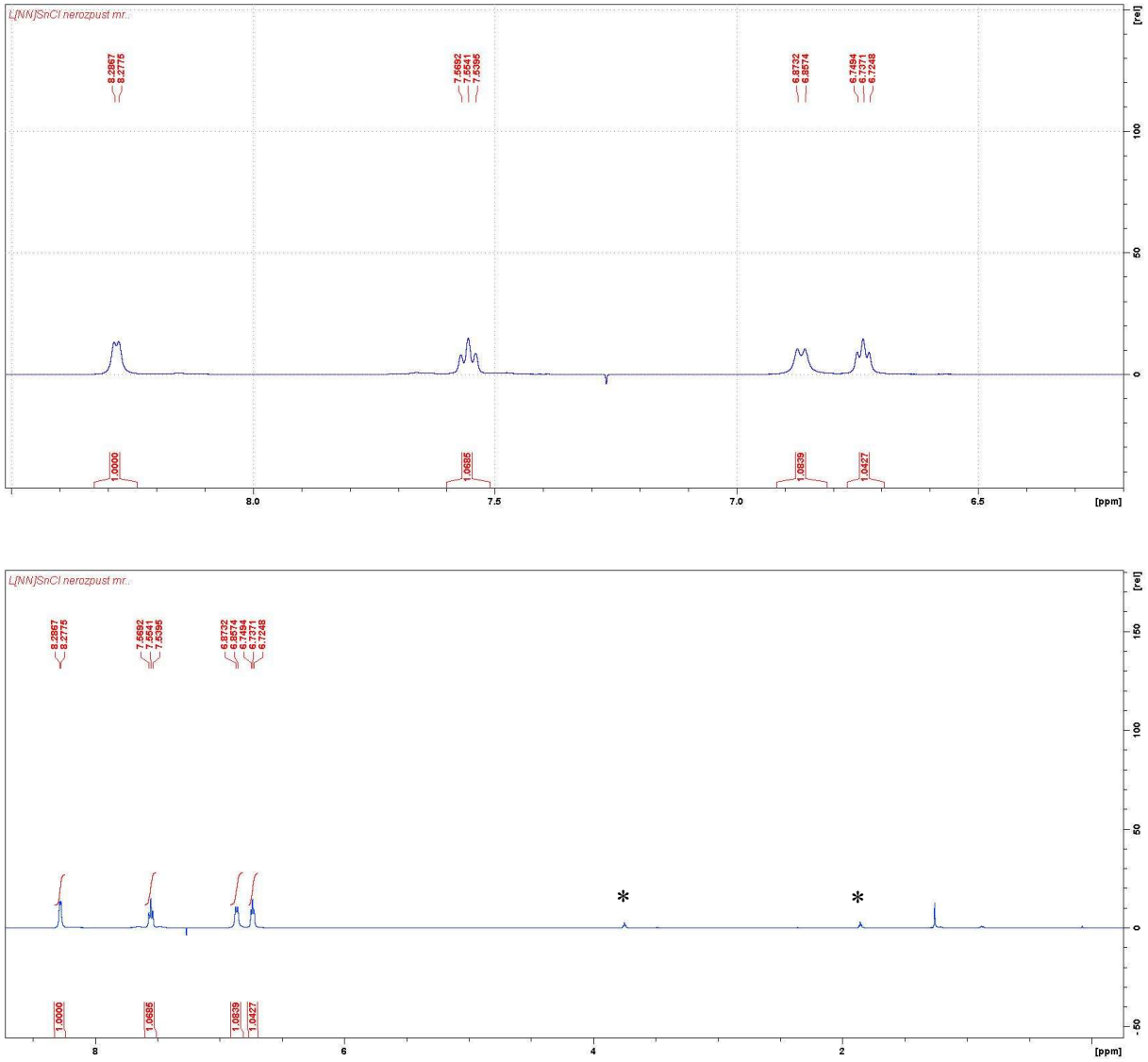

Figure S6: ^{1}H NMR spectrum of **4** in $CDCl_3$ (* traces of thf).

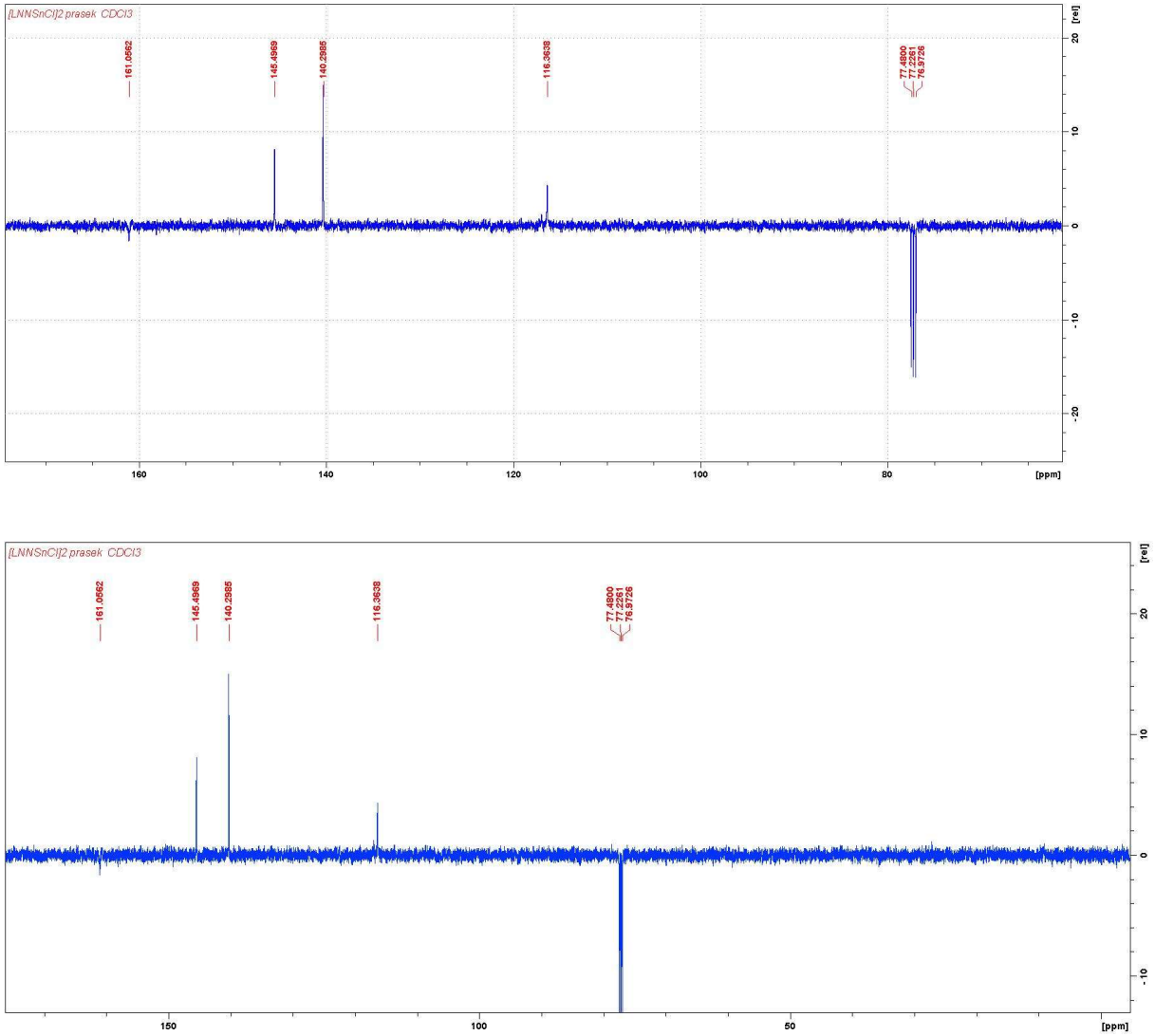

Figure S7: $^{13}C\{^{1}H\}$-APT NMR spectrum of **4** in $CDCl_3$.

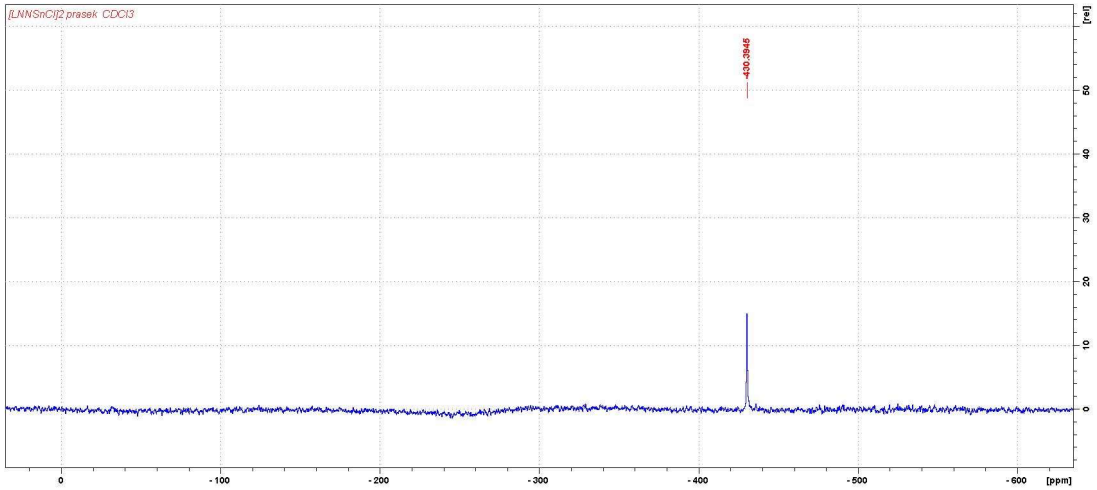

Figure S8: $^{119}Sn\{^{1}H\}$ NMR spectrum of **4** in $CDCl_3$.

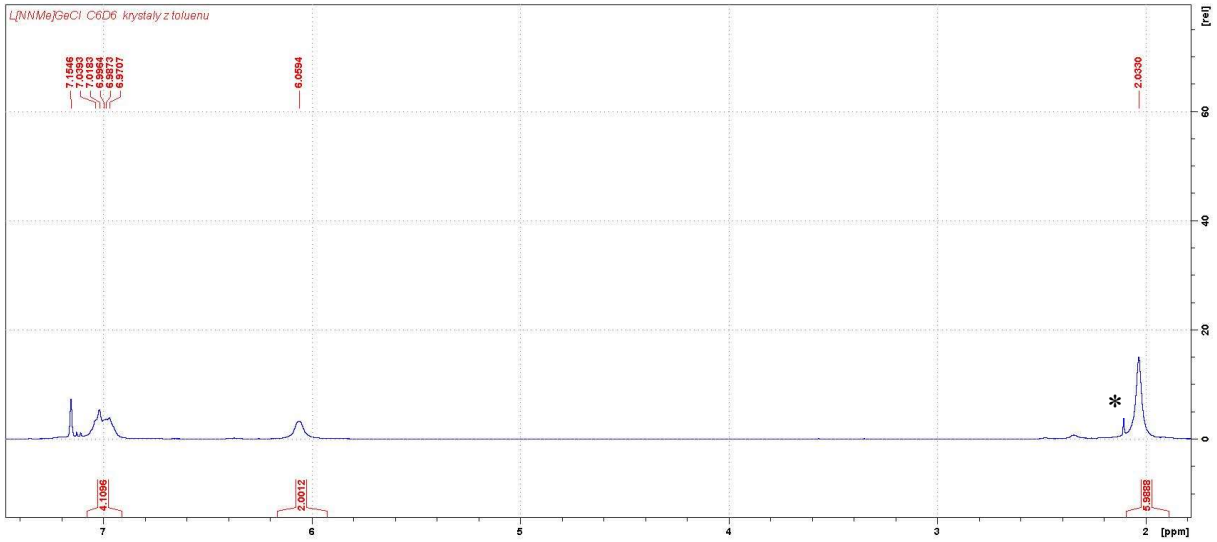

Figure S9: ^{1}H NMR spectrum of **5** in C_6D_6 (* traces of toluene).

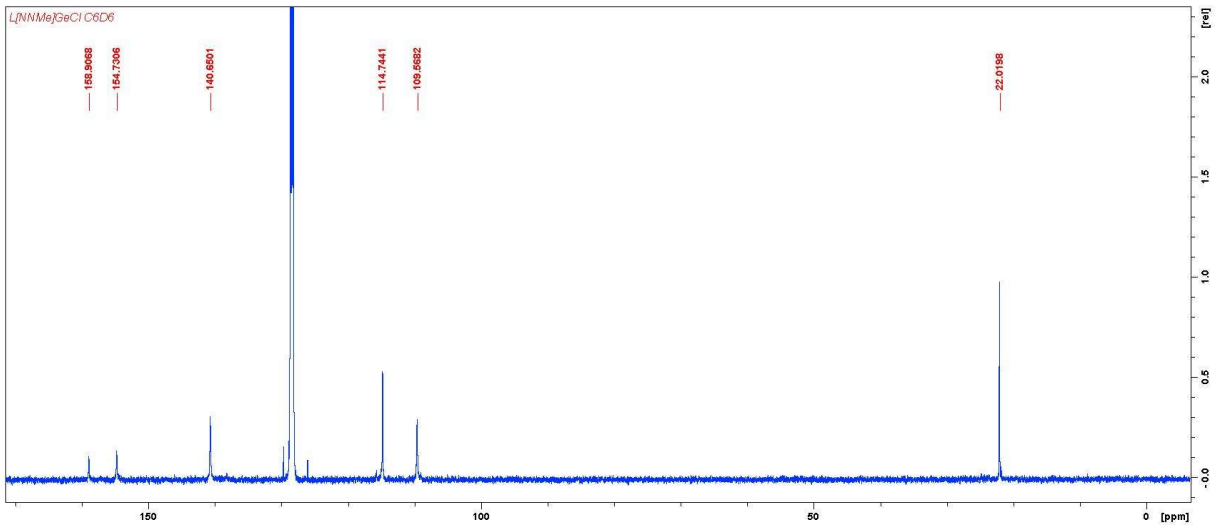

Figure S10: $^{13}C\{^{1}H\}$ NMR spectrum of **5** in C_6D_6.

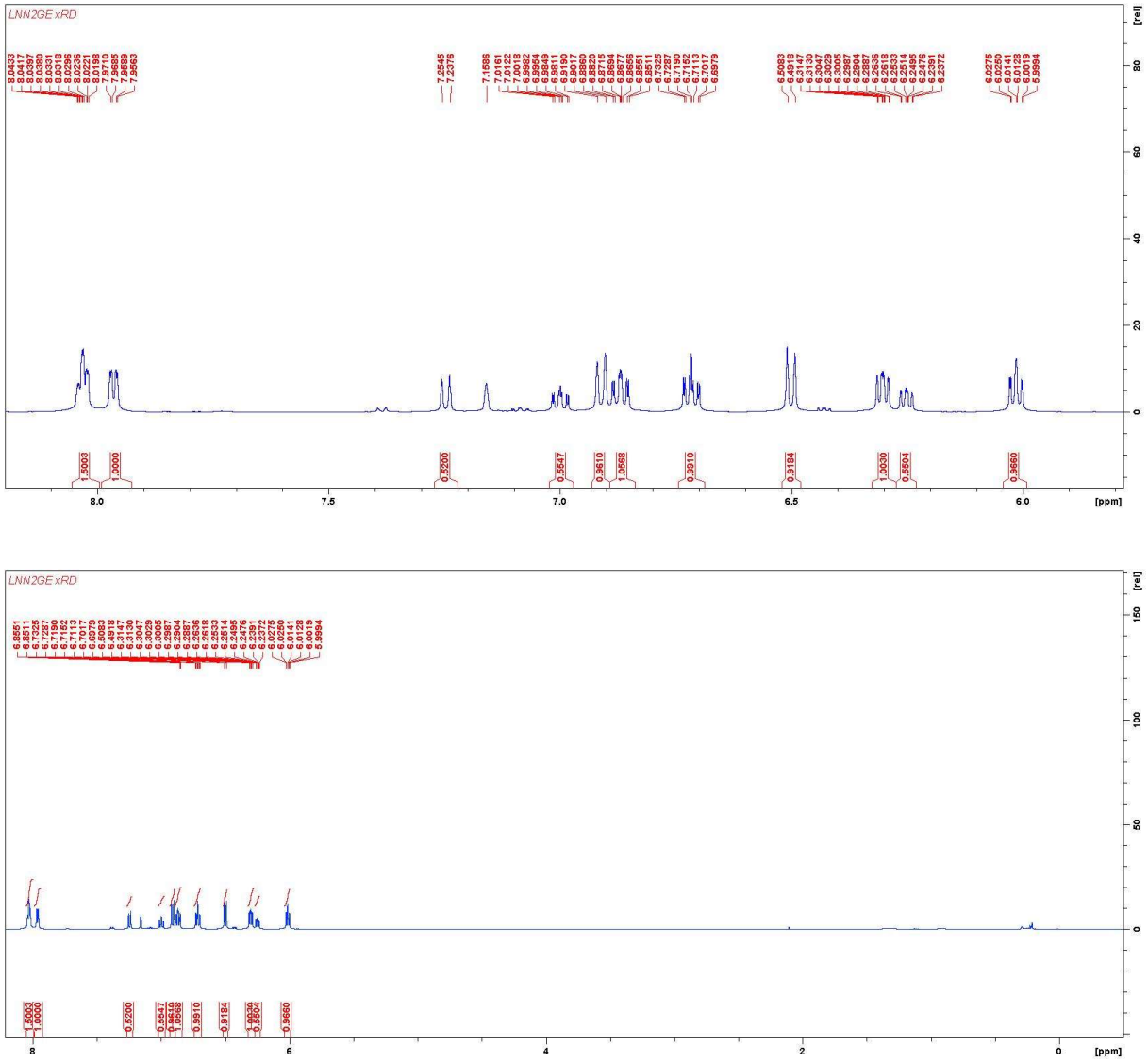

Figure S11: ^{1}H NMR spectrum of **6** in C_6D_6.

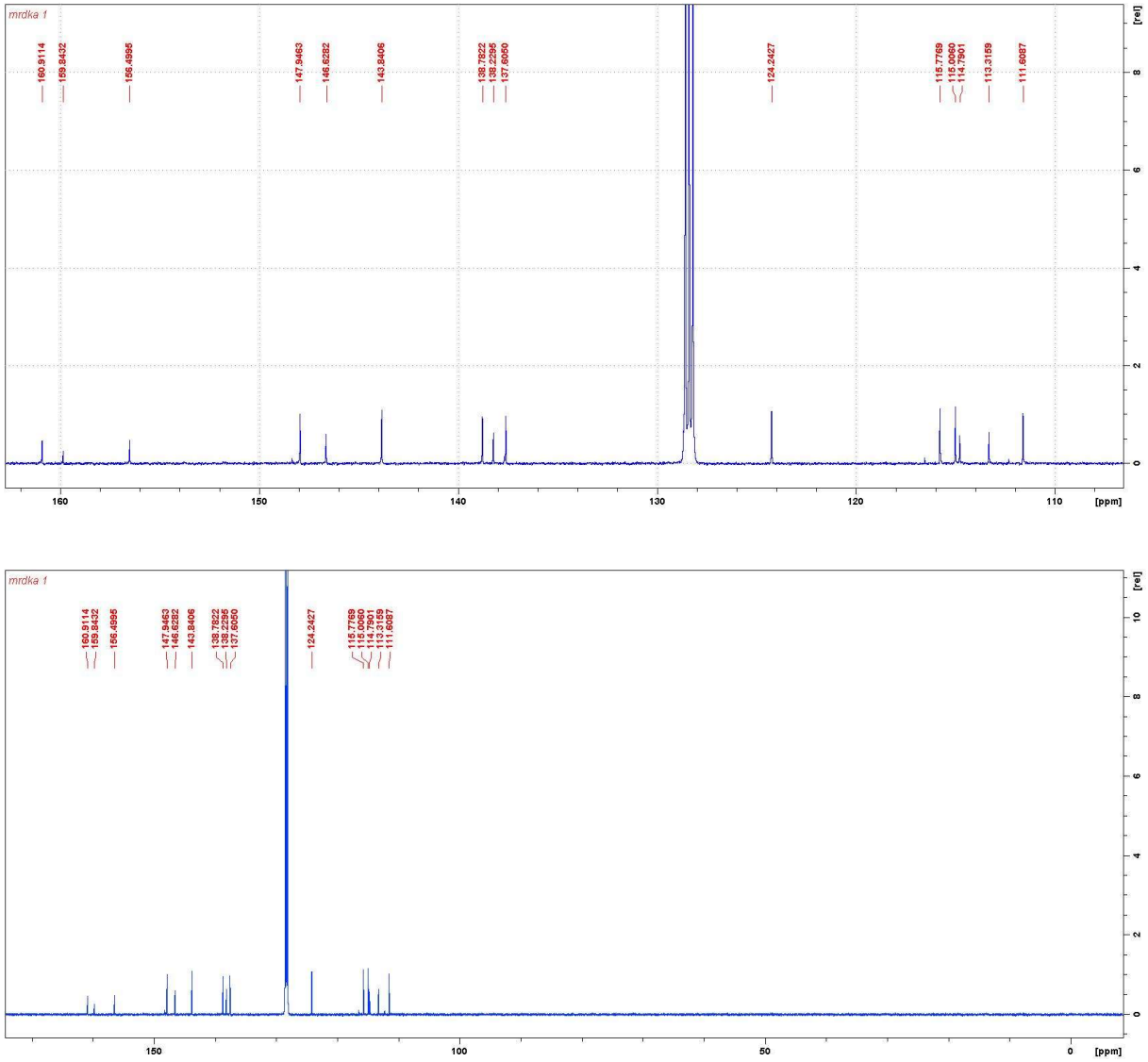

Figure S12: $^{13}C\{^{1}H\}$ NMR spectrum of **6** in C_6D_6.

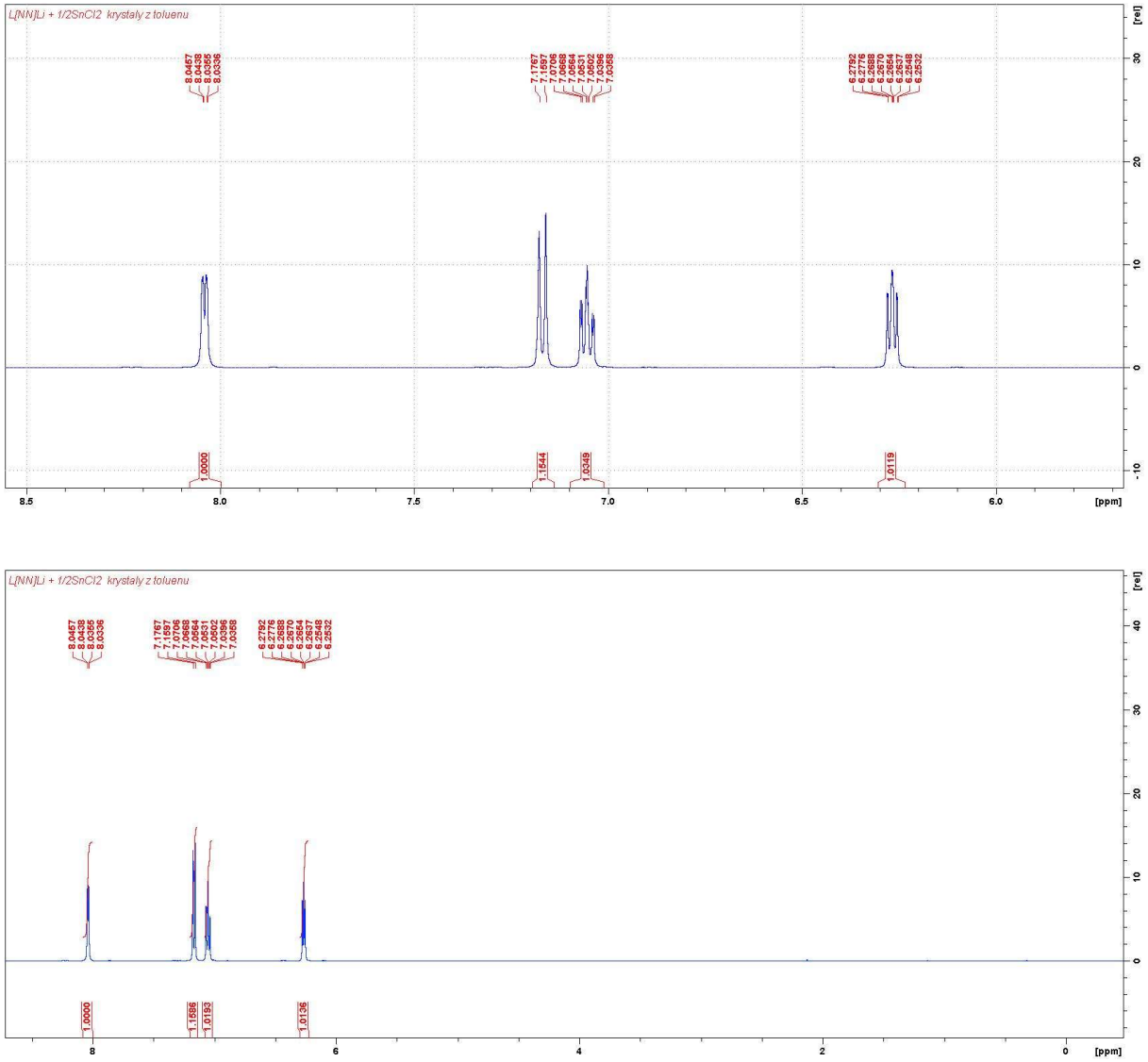

Figure S13: ^{1}H NMR spectrum of **7** in C_6D_6.

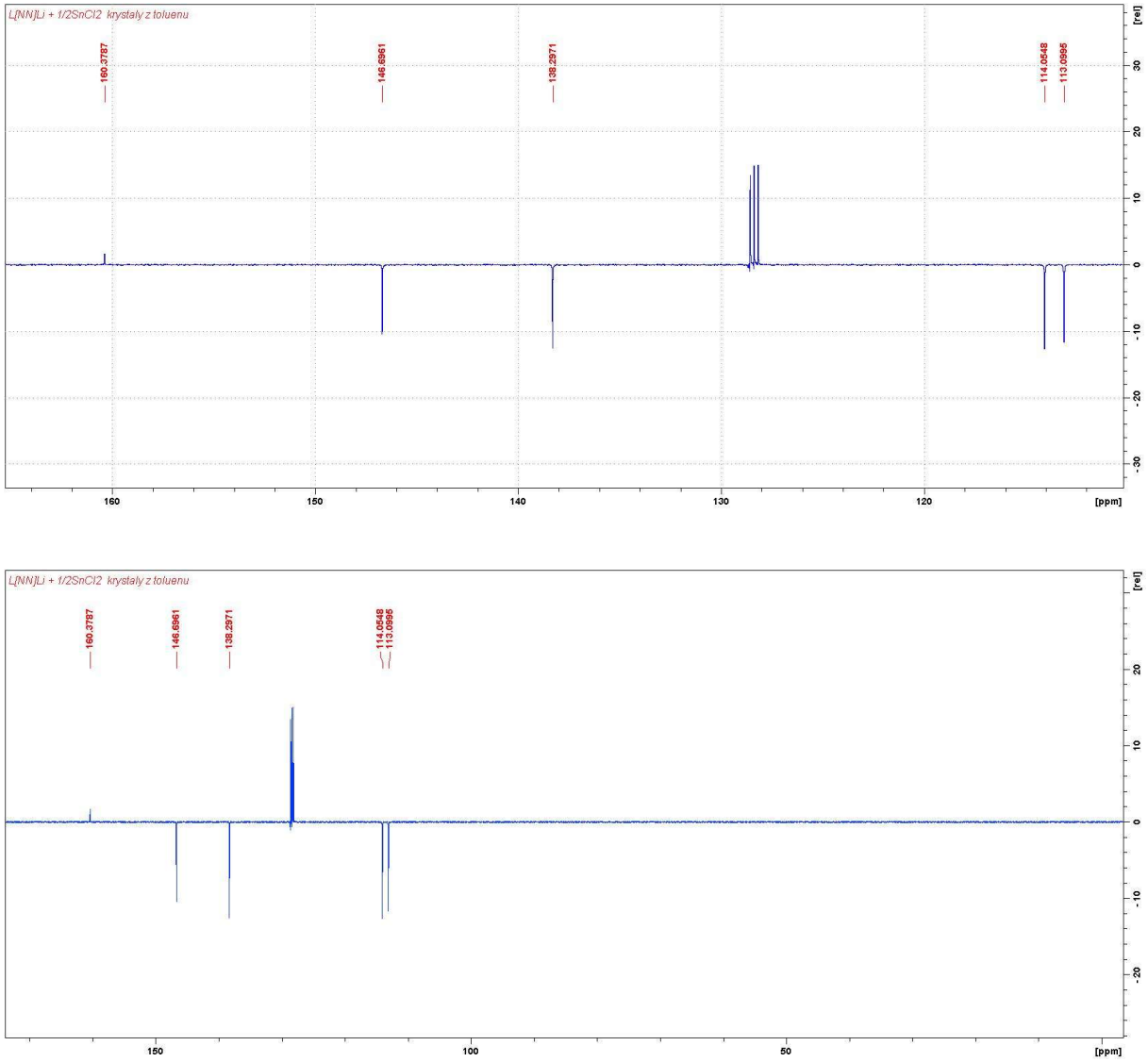

Figure S14: $^{13}C\{^{1}H\}$ - APT NMR spectrum of **7** in C_6D_6.

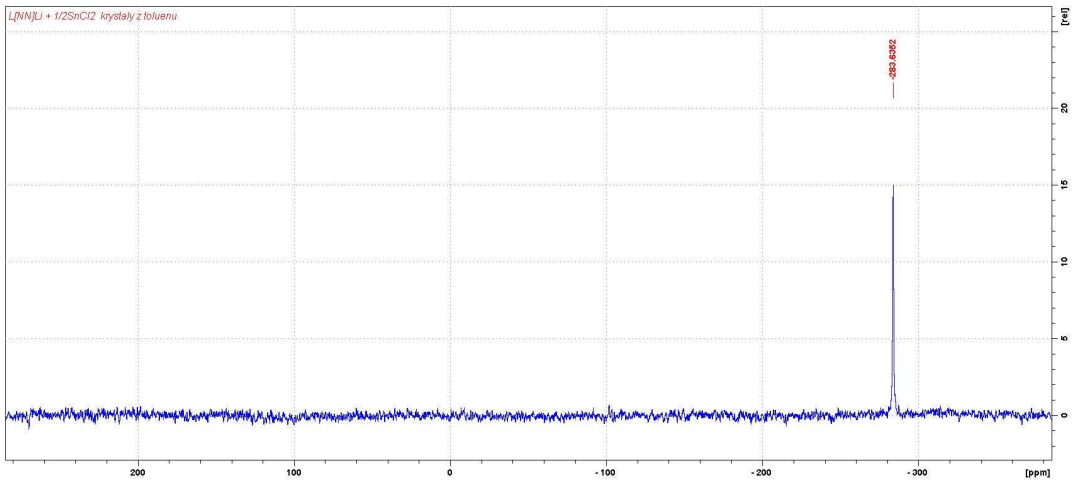

Figure S15: $^{119}Sn\{^{1}H\}$ NMR spectrum of **7** in C_6D_6.

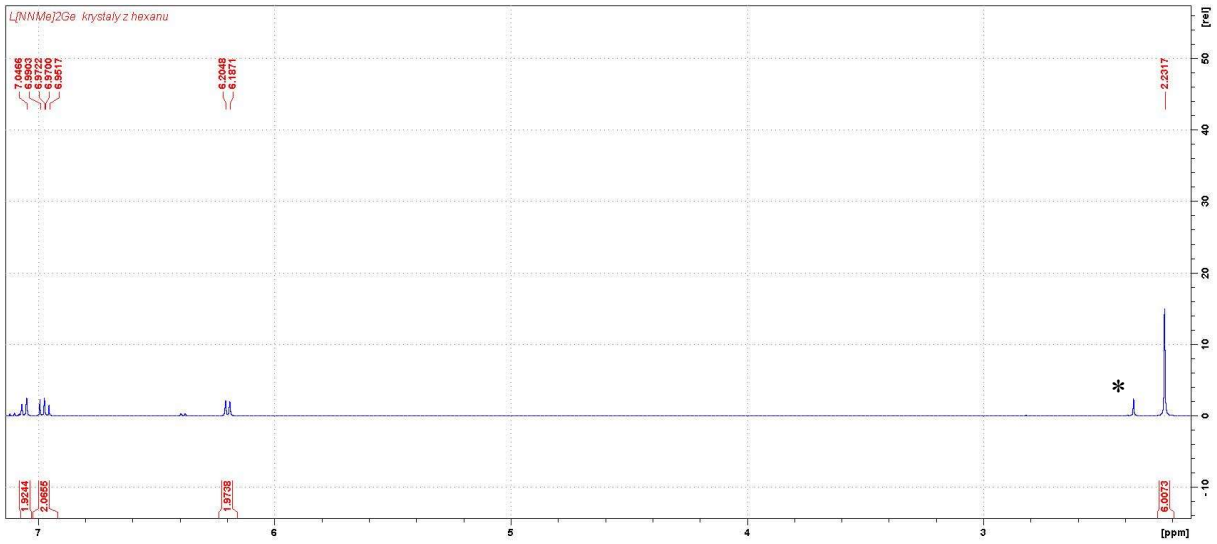

Figure S16: ^{1}H NMR spectrum of **8** in C_6D_6 (*unknown impurity).

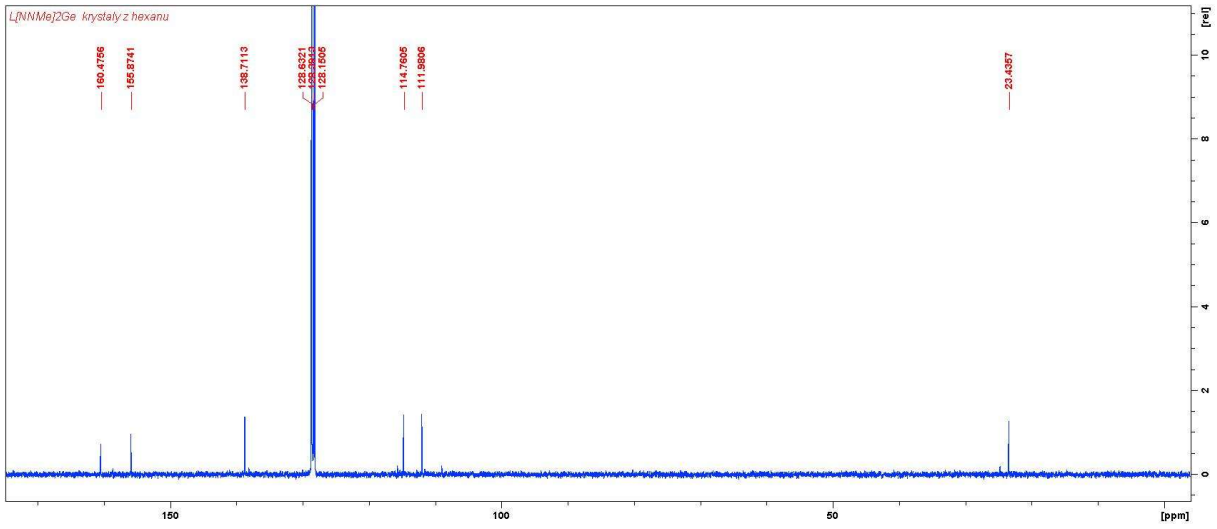

Figure S17: $^{13}C\{^{1}H\}$ NMR spectrum of **8** in C_6D_6.

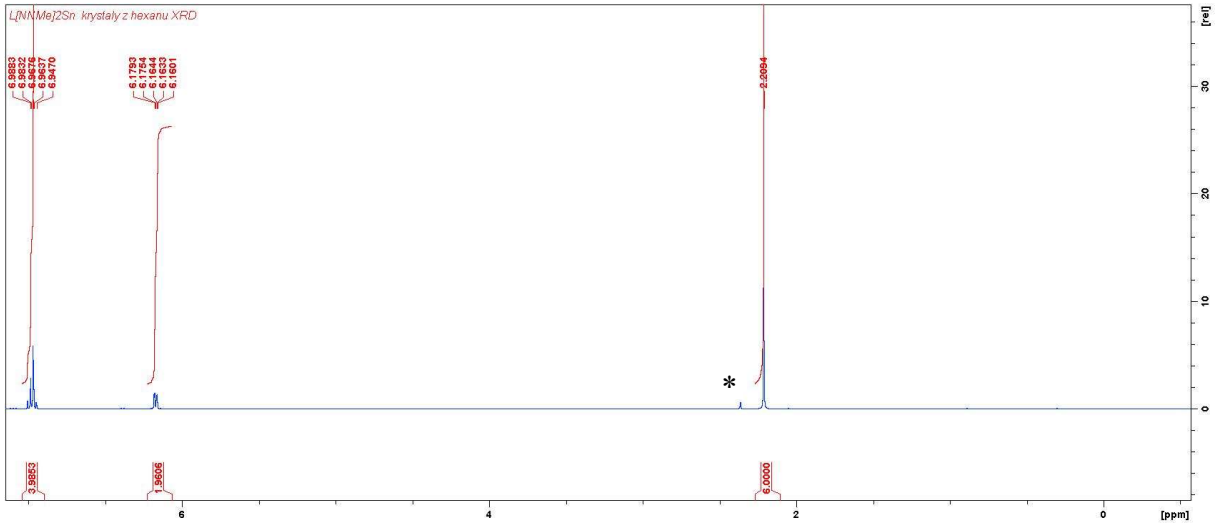

Figure S18: ^{1}H NMR spectrum of **9** in C_6D_6 (*unknown impurity).

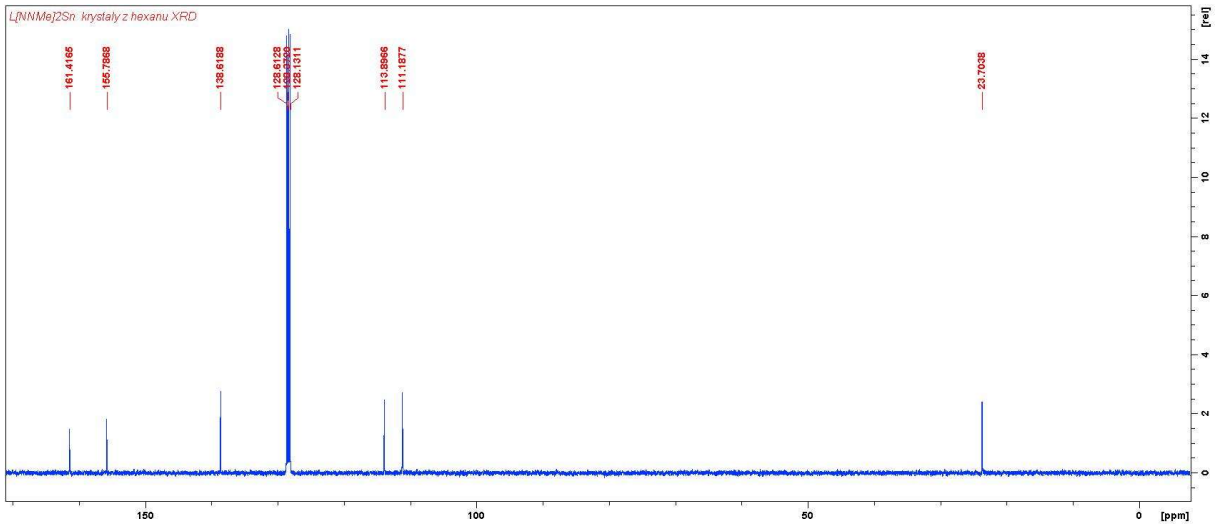

Figure S19: $^{13}C\{^{1}H\}$ NMR spectrum of **9** in C_6D_6.

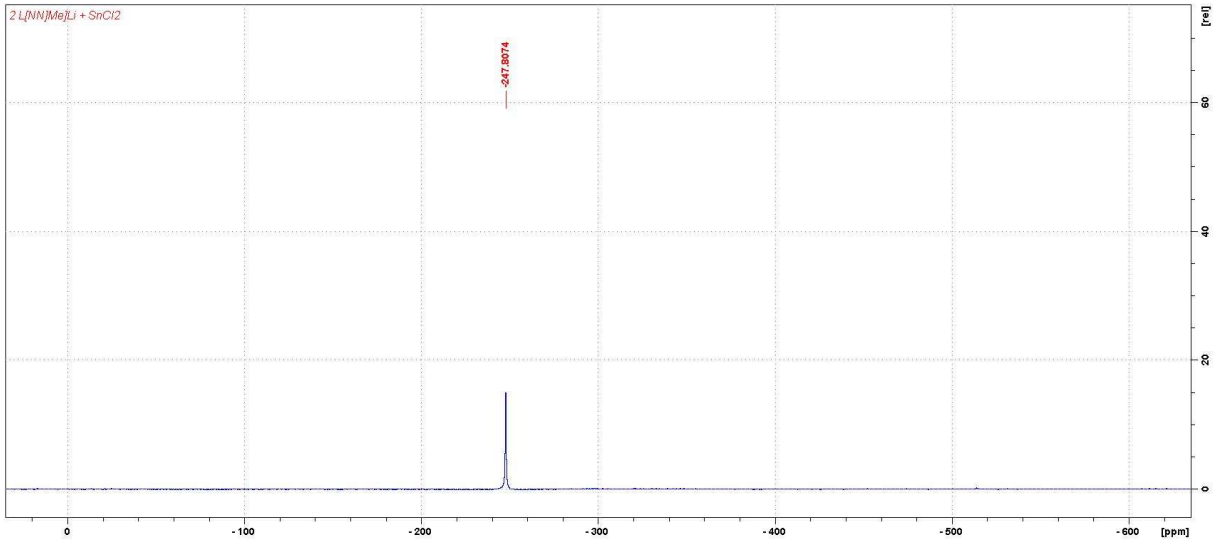

Figure S20: $^{119}Sn\{^{1}H\}$ NMR spectrum of **9** in C_6D_6.

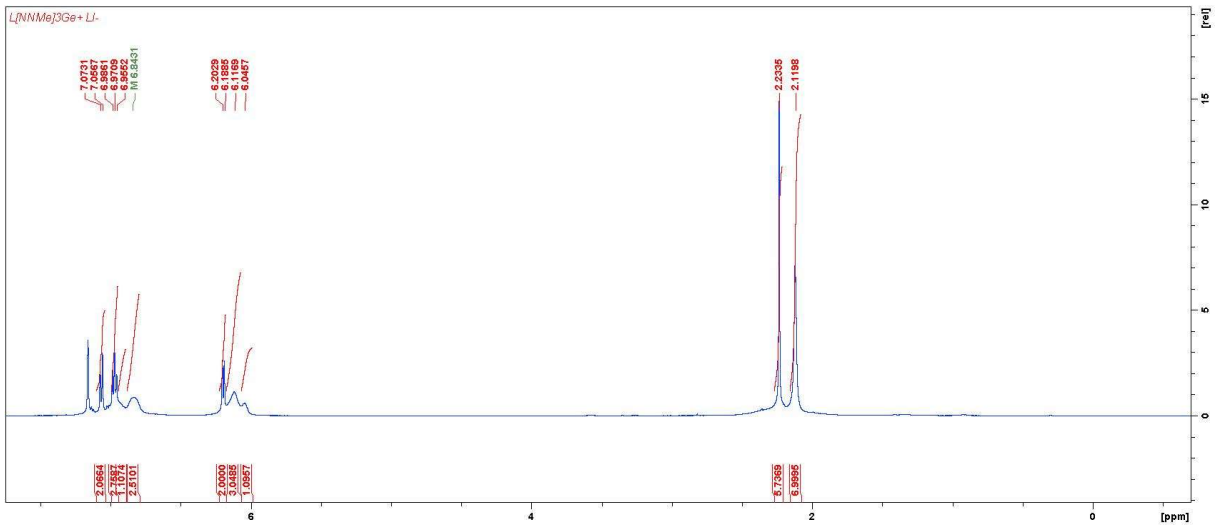

Figure S21: ^{1}H NMR spectrum of **10** in C_6D_6.

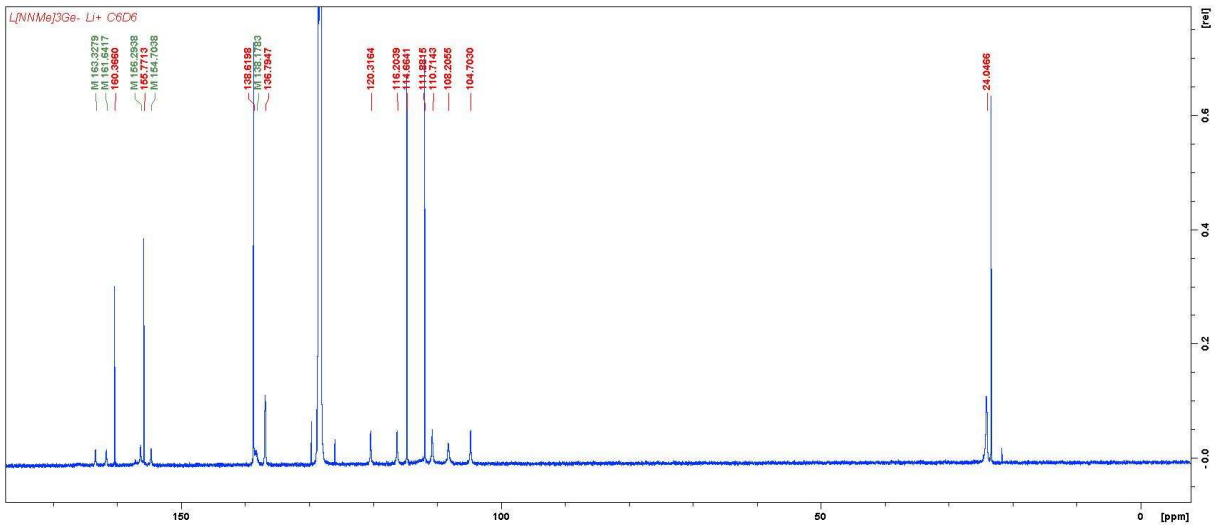

Figure S22: $^{13}C\{^{1}H\}$ NMR spectrum of **10** in C_6D_6.

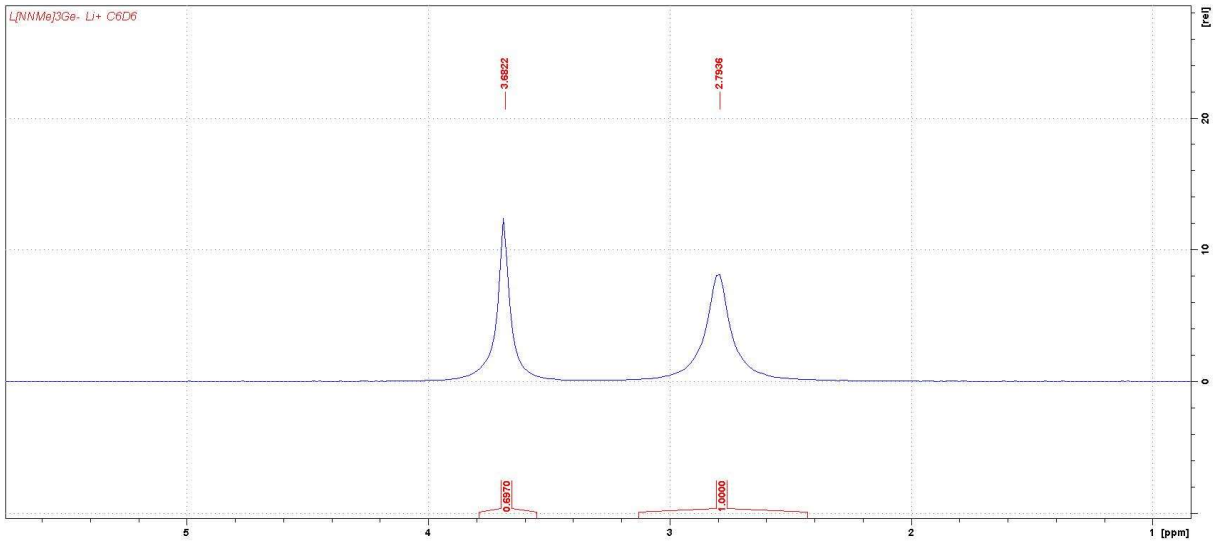

Figure S23: $^{7}Li\{^{1}H\}$ NMR spectrum of **10** in C_6D_6.

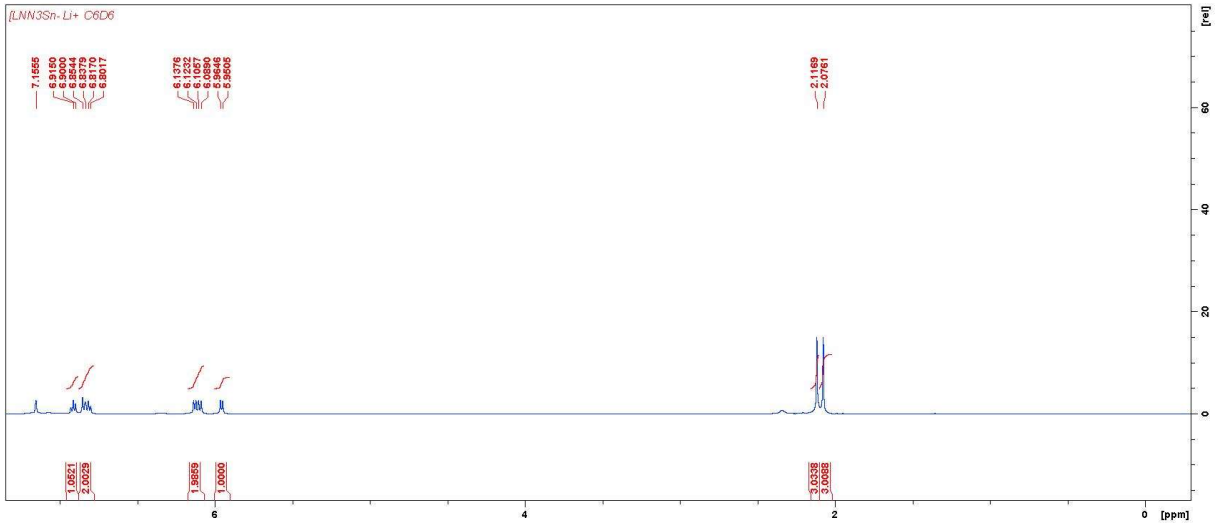

Figure S24: ^{1}H NMR spectrum of **11** in C_6D_6.

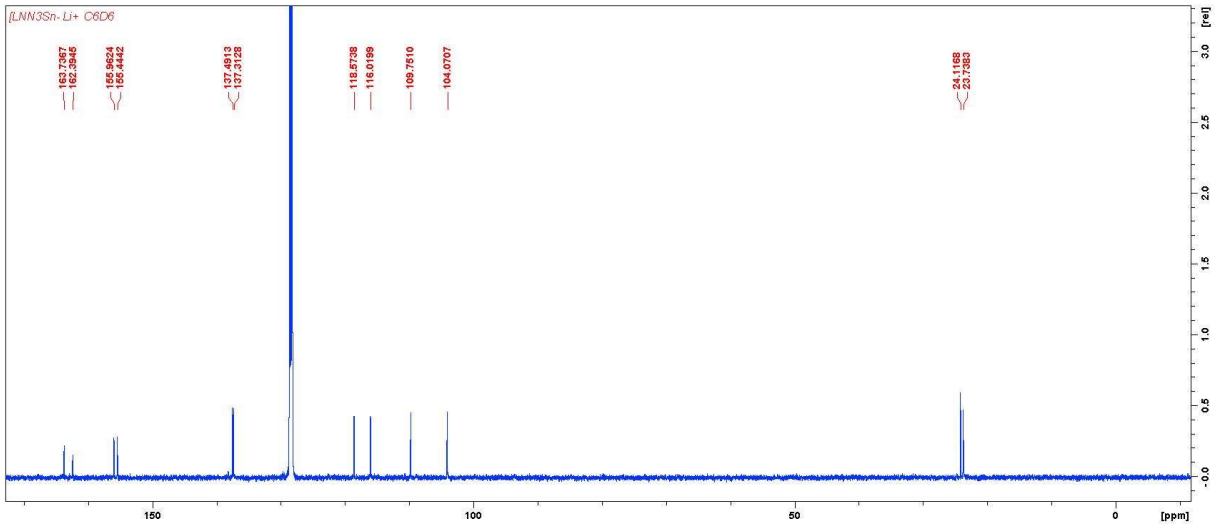

Figure S25: $^{13}C\{^{1}H\}$ NMR spectrum of **11** in C_6D_6.

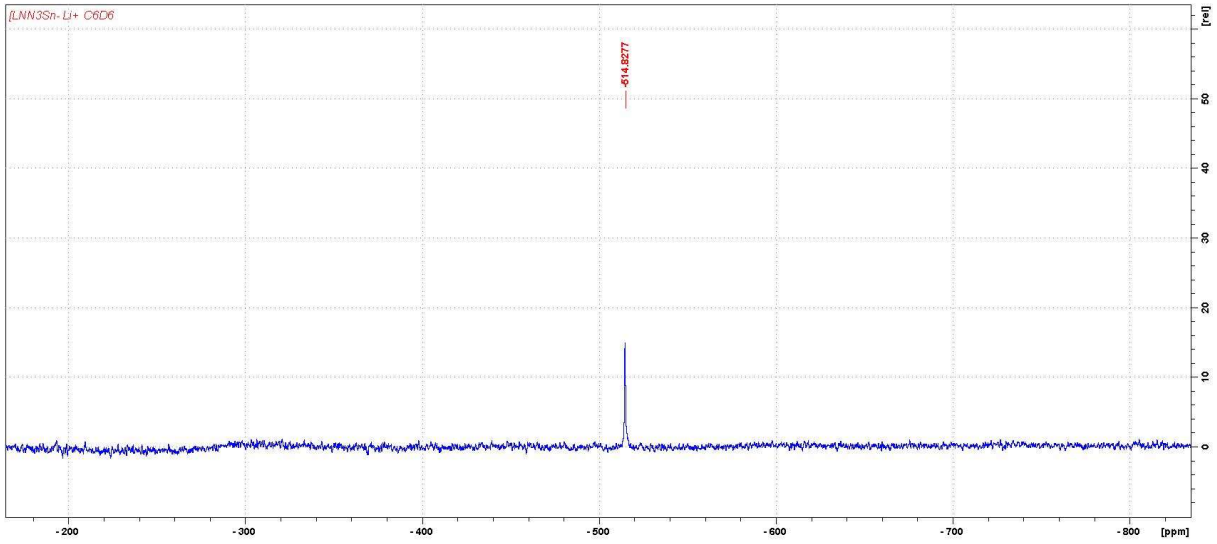

Figure S26: $^{119}Sn\{^{1}H\}$ NMR spectrum of **11** in C_6D_6.

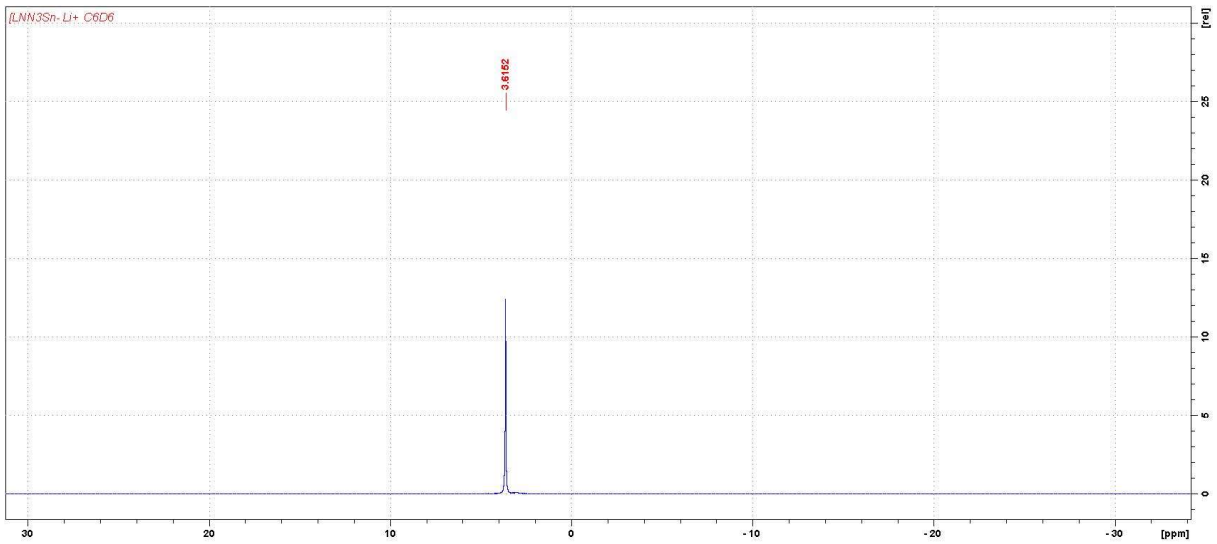

Figure S27: $^{7}Li\{^{1}H\}$ NMR spectrum of **11** in C_6D_6.

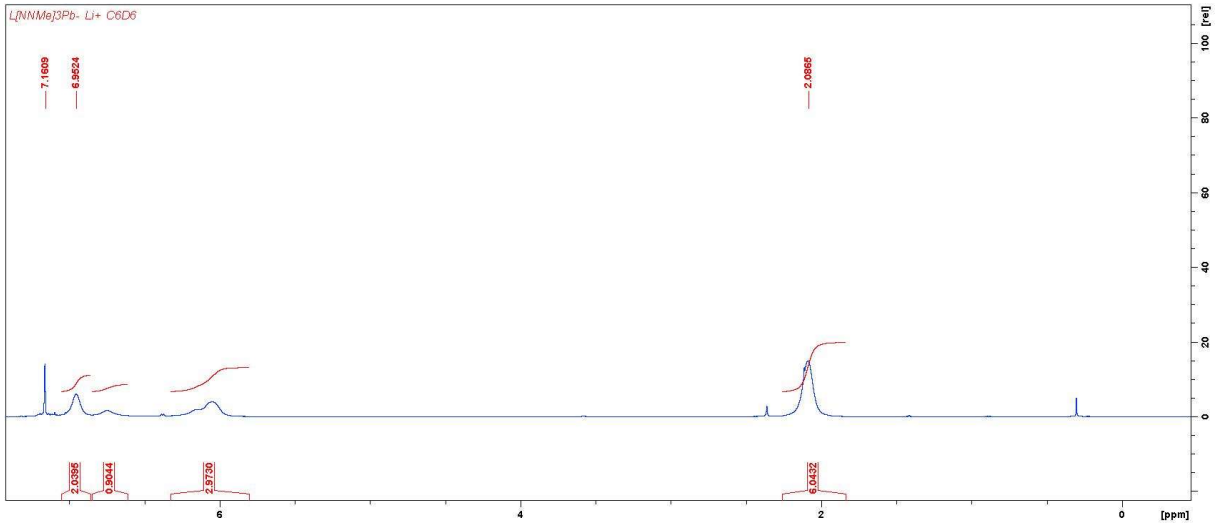

Figure S28: ^{1}H NMR spectrum of **12** in C_6D_6.

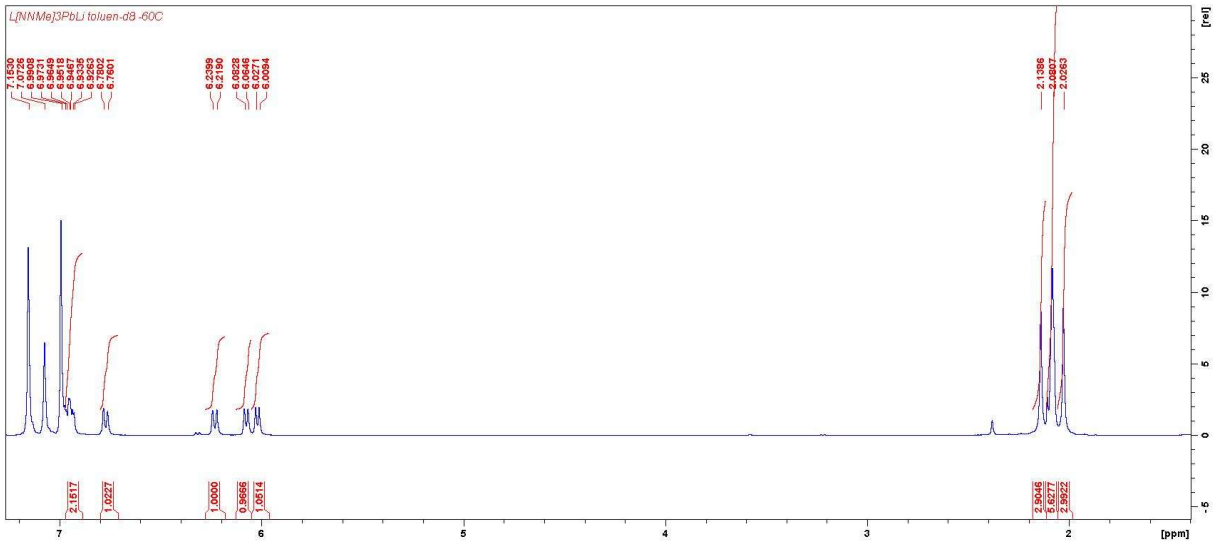

Figure S29: ^{1}H NMR spectrum of **12** in toluene-d8 -60°C.

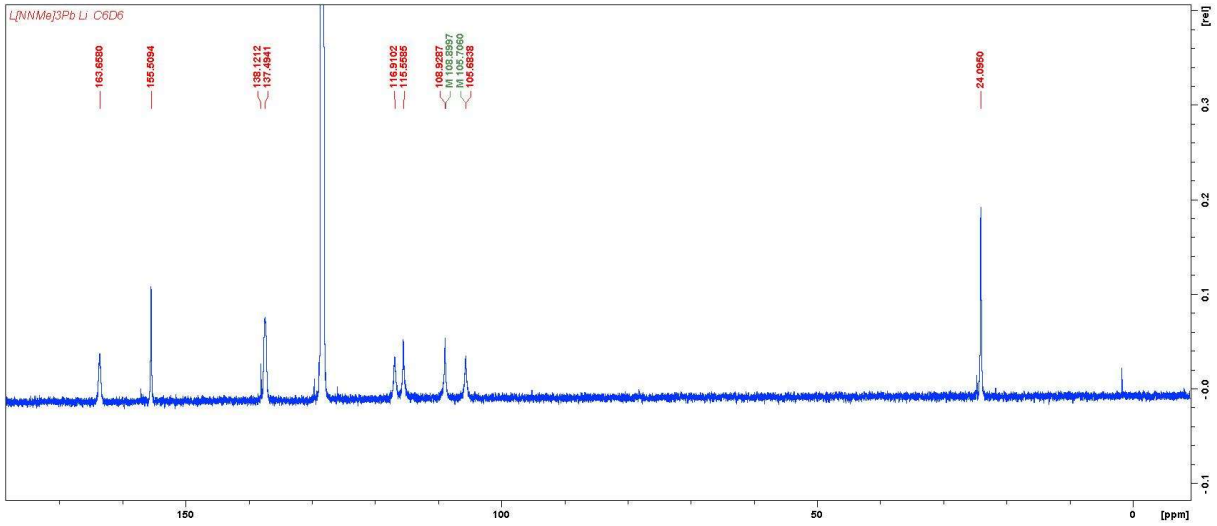

Figure S30: $^{13}C\{^{1}H\}$ NMR spectrum of **12** in C_6D_6.

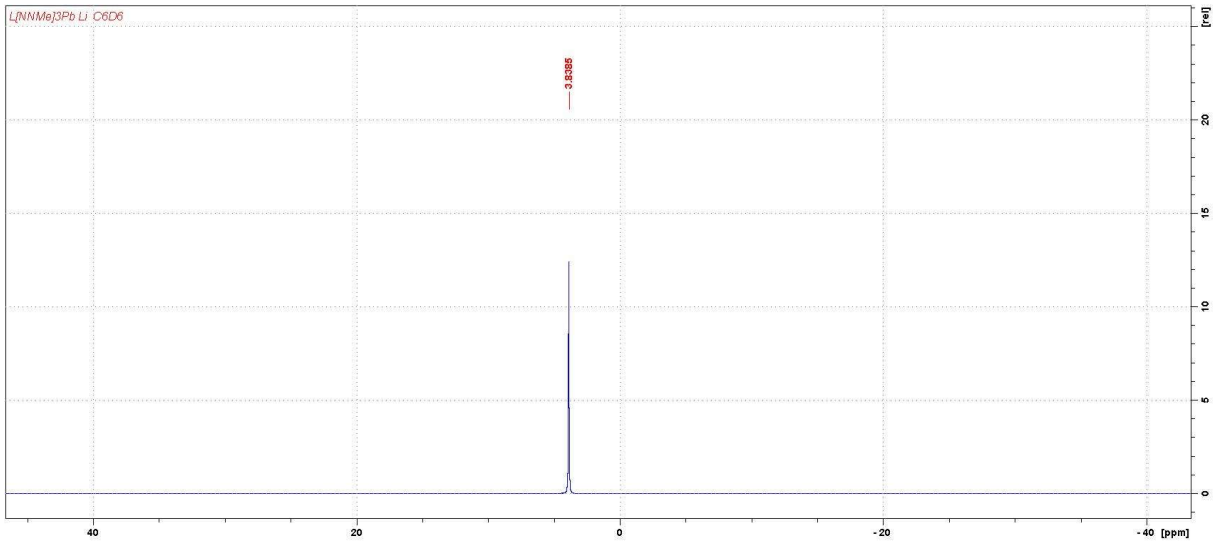

Figure S31: $^{7}Li\{^{1}H\}$ NMR spectrum of **12** in C_6D_6.

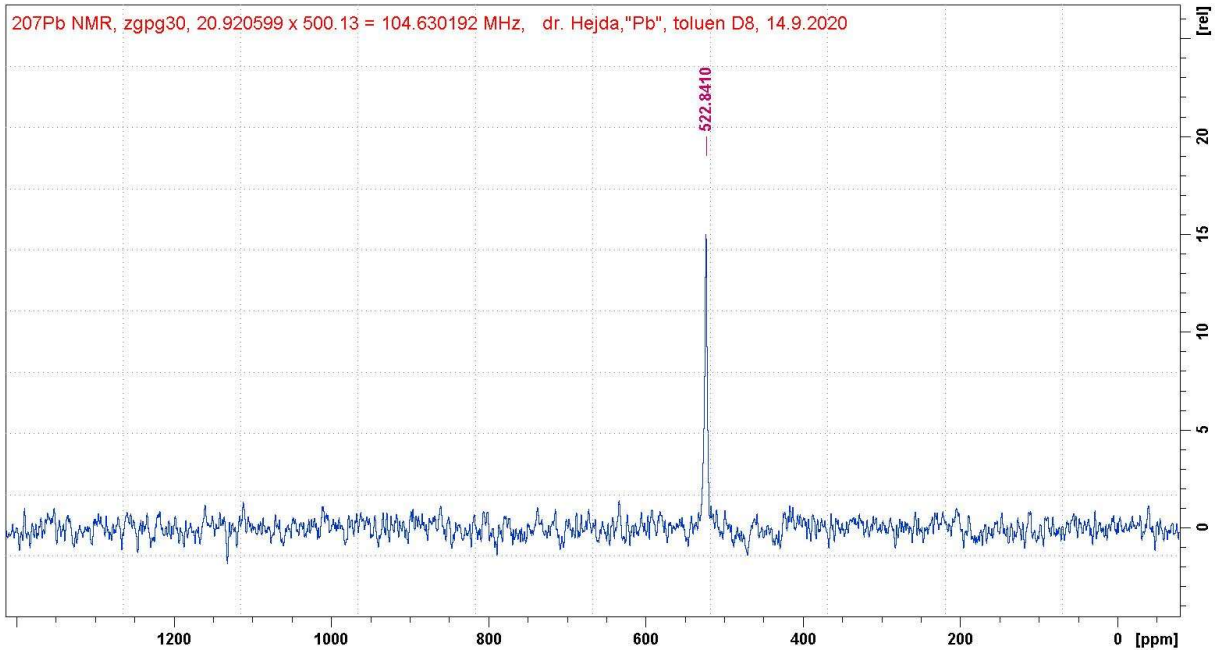

Figure S32: $^{207}Pb\{^{1}H\}$ NMR spectrum of **12** in C_6D_6.

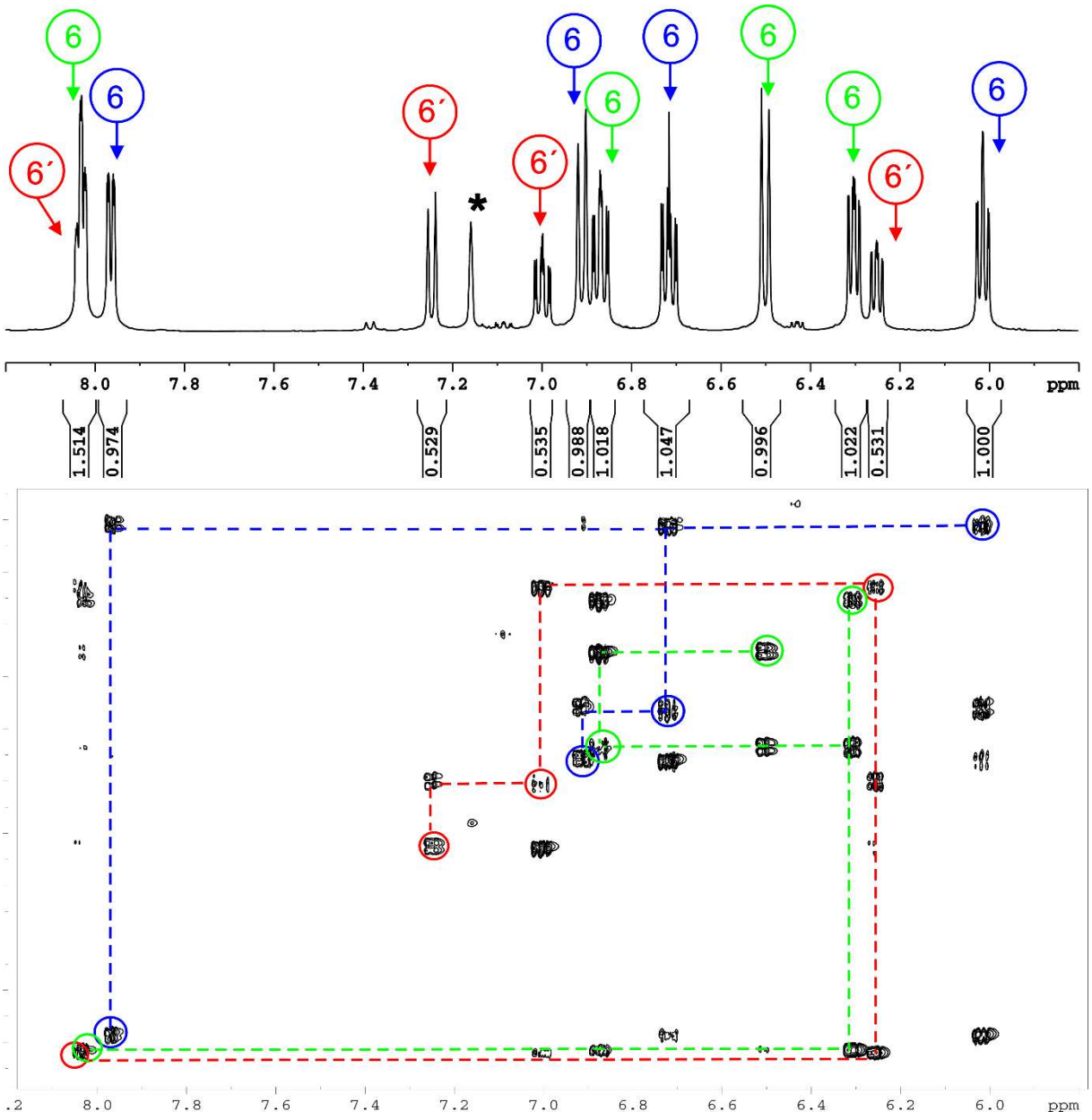

Figure S33: ^{1}H, ^{1}H COSY NMR spectrum of **6** in C_6D_6 (*) illustrating the presence of two isomers **6** and **6´** in solution at r.t.

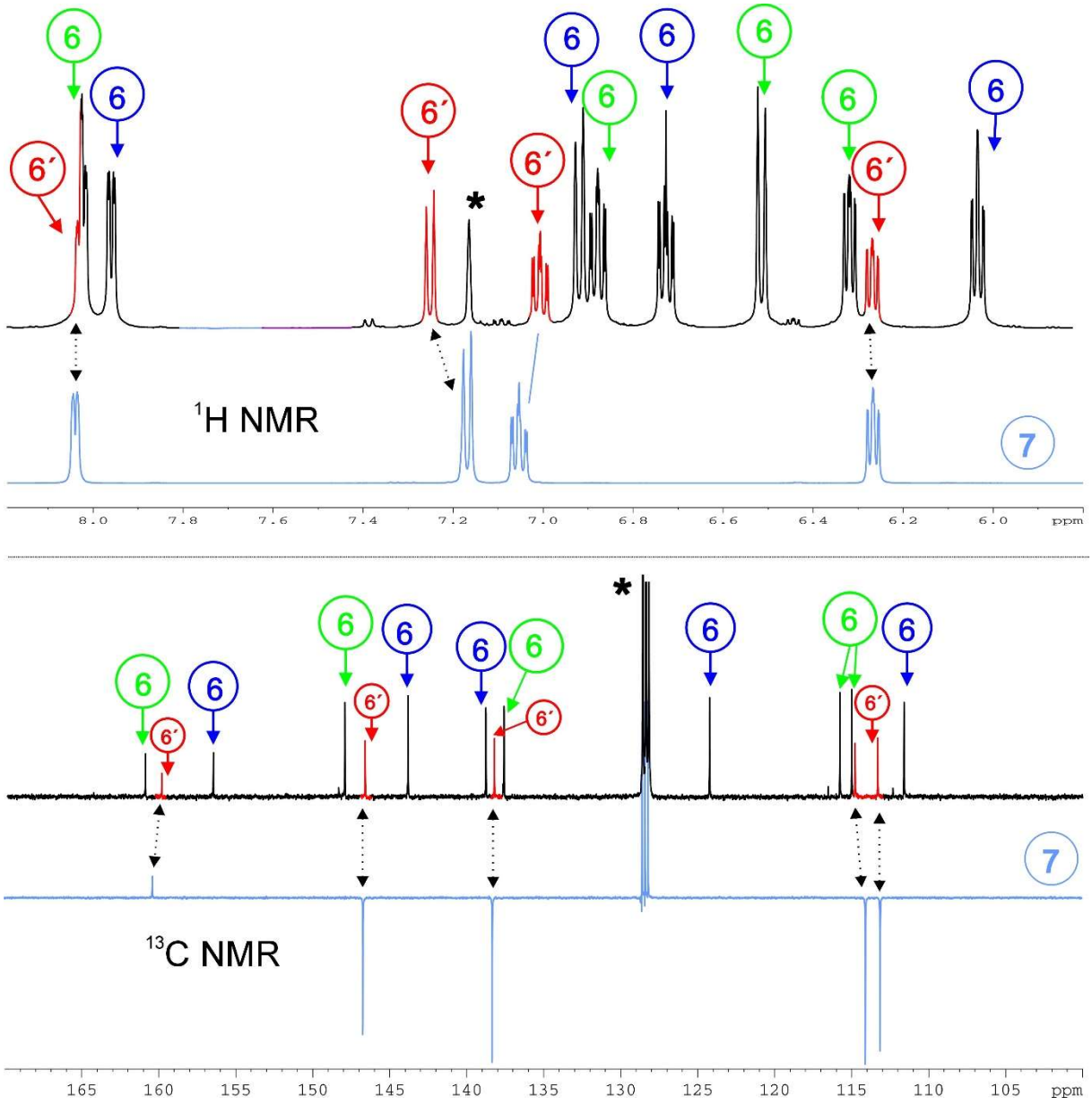

Figure S34: Comparison of ^{1}H and ^{13}C{^{1}H} NMR spectra stannylene **7** and mixture of two isomers germylene **6** and **6´** in C_6D_6 (*) showing a close resemblance between **7** and **6´**.

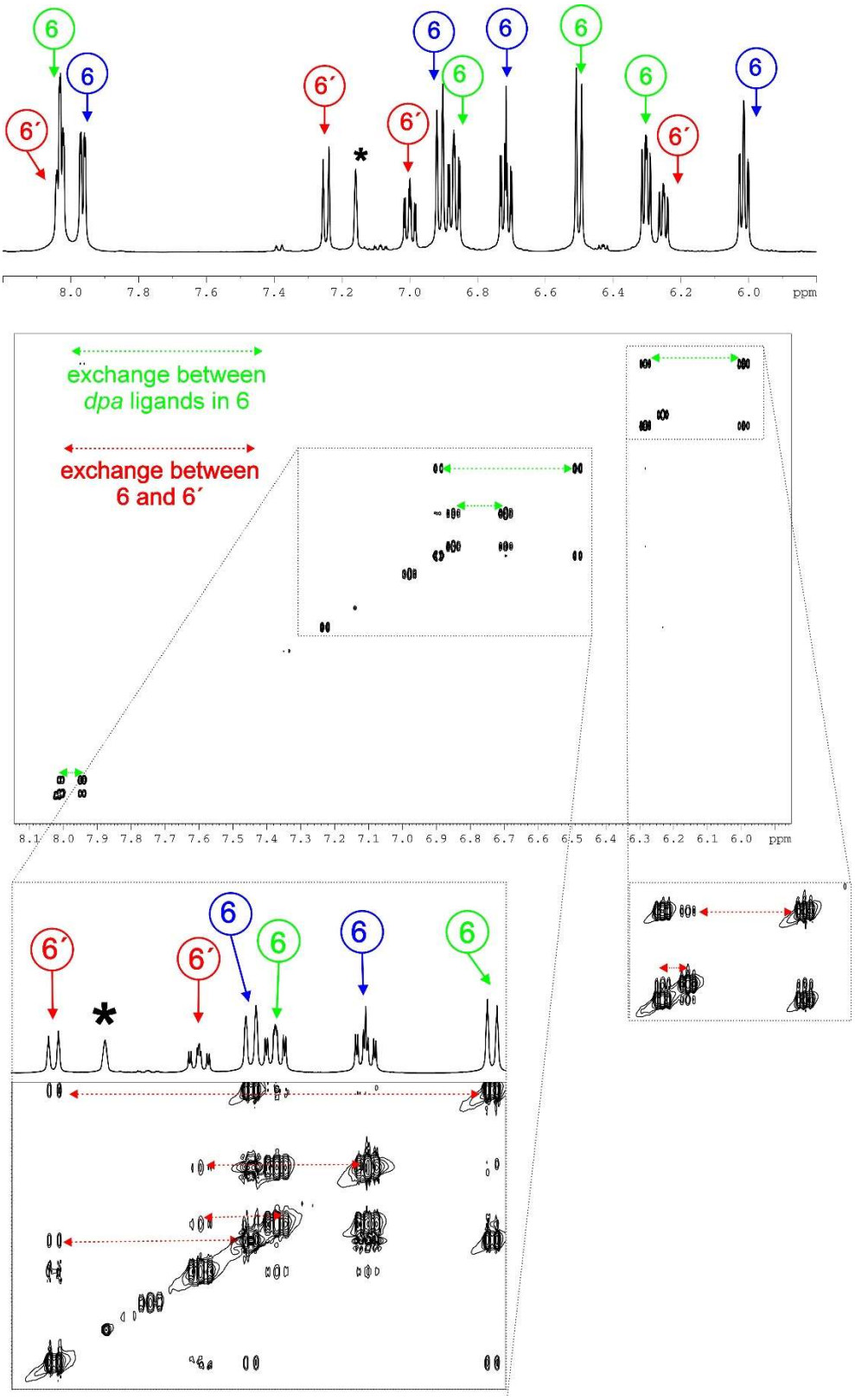

Figure S35: ^{1}H, ^{1}H EXSY NMR spectrum of of **6** in C_6D_6 (*) showing a mutual dynamic exchange between both *dpa* ligands in **6** (green) and their exchange with the proposed second isomer **6´** (red). Note that all marked cross-peaks are in the same phase as the diagonal peaks.

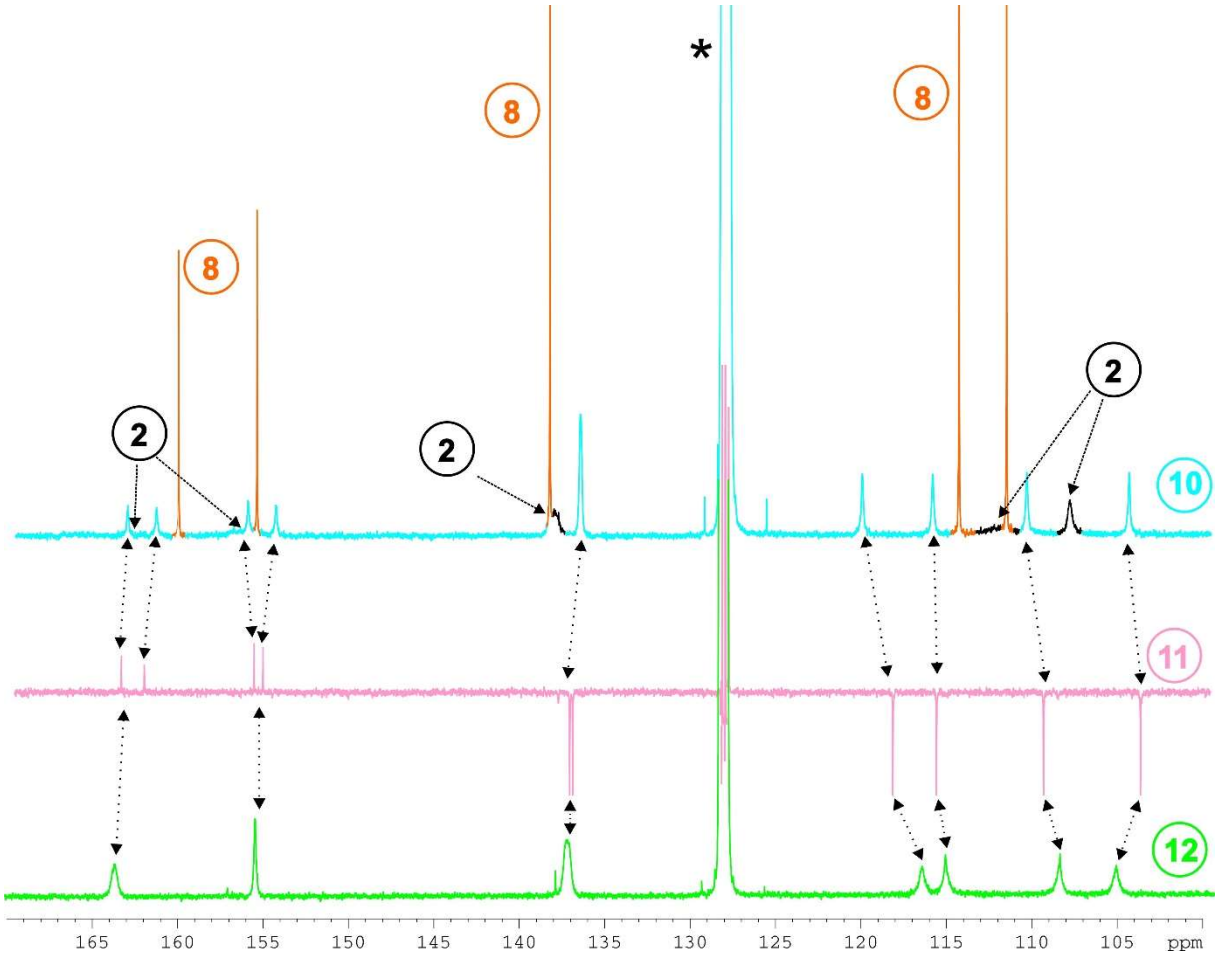

Figure S36: Comparison of $^{13}C\{^{1}H\}$ NMR spectra of **10-12** in C_6D_6 (*) showing a mutual resemblance between **10 - 12** (in the case of **12** some resonances seem to be overlapped). Furthermore, a mixture obtained upon dissolution of single crystals of **10** (top) containing besides signals of **10** those of germylene **8** and lithium derivative **2** as a result of partial decomposition of **10** in solution. Please note that some signals of **2** are not resolved due their significant broadening, please see also $^{13}C\{^{1}H\}$ NMR spectrum of isolated **2** showing a very broaden resonances (Figure S2).

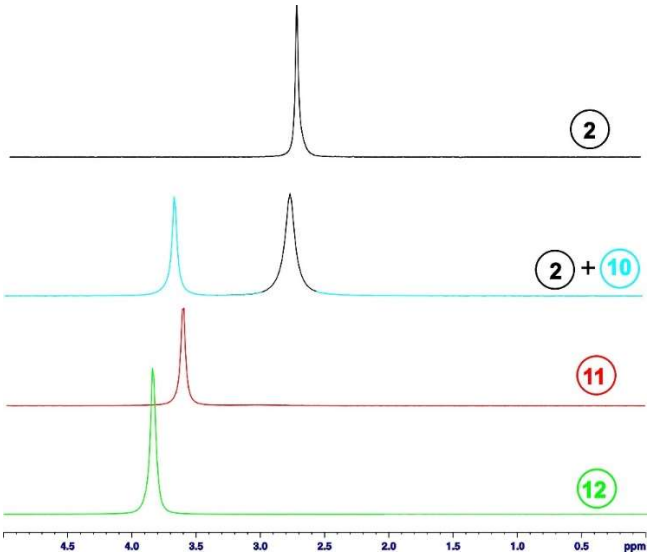

Figure S37: Comparison of $^{7}Li\{^{1}H\}$ NMR spectra of **10**-**12** in C_6D_6 (*) showing a mutual resemblance between **11** and **12**. Furthermore, a mixture of two components obtained upon dissolution of single crystals of **10** containing besides signals of **10** that of the lithium derivative **2** as a result of partial decomposition of **10** in solution is presented. The $^{7}Li\{^{1}H\}$ NMR spectrum of pure **2** is also included.

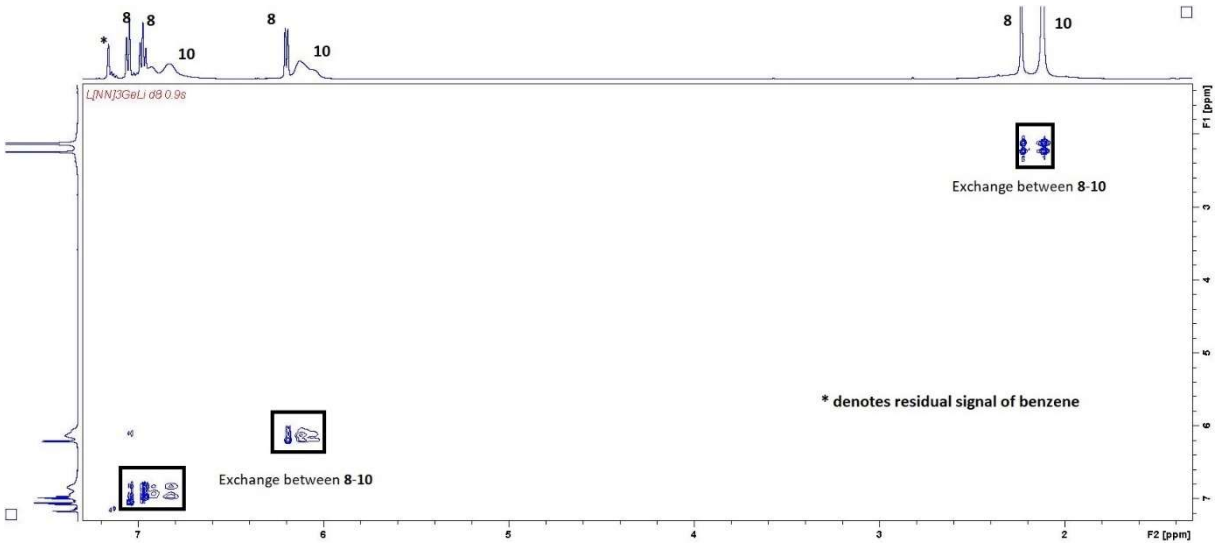

Figure S38: ^{1}H, ^{1}H EXSY NMR spectrum of dissolved single crystals of **10** in C_6D_6 (*) showing a mutual dynamic exchange between **10** (blue) and the germylene **8** (orange). The exchange with the lithium complex **2** is not resolved probably due a significant broadening of the signals. Note that all marked cross-peaks are in the same phase as the diagonal peaks.

2. Crystallographic data.

Table S1. Crystal data and structure refinement of studied compounds.

	2	**3**	**4**
Formula	$C_{48}H_{48}Li_4N_{12}$	$C_{10}H_8ClGeN_3$	$C_{20}H_{16}Cl_2N_6Sn_2$
Formula weight, g mol^{-1}	662.28	278.23	648.67
Crystal system	Triclinic	Triclinic	Orthorhombic
Crystal size, mm	0.44 × 0.25 × 0.13	0.59 × 0.38 × 0.20	0.20 × 0.19 × 0.16
Space group	P-1	P-1	$Pca2_1$
a, Å	11.1572(4)	8.2653(5)	17.1415(8)
b, Å	11.5648(4)	9.9478(6)	8.3019(4)
c, Å	19.6657(7)	12.6110(7)	14.9727(6)
α, º	79.294(2)	91.910(3)	90
β, º	76.670(2)	92.733(3)	90
γ, º	62.192(2)	91.899(3)	90
V, Å^3	2174.94(14)	1034.51(11)	2130.72(11)
Z	2	4	4
ρ_{calcd}, Mg m^{-3}	1.253	1.982	2.022
μ (Mo $K\alpha$), mm^{-1}	0.593	3.185	2.616
F(000)	864	552	1248
θ range, deg	1 to 27.5	1 to 27.5	1 to 27.5
No. of reflns collected	52110	30605	19086
No. indep. Reflns	9155	4750	4850
No. obsd reflns with ($I>2\sigma(I)$), R_{int}	4900, 0.1578	3956, 0.037	3907, 0.60
No. refined params	586	271	272
GooF (F^2)	1.297	1.025	1.027
R_1 (F) ($I > 2\sigma(I)$)	0.1095	0.0295	0.0373
wR_2 (F^2) (all data)	0.2443	0.0676	0.0793
Largest diff peak/hole, e Å^{-3}	0.648 / –0.691	0.693 / –0.679	2.453 / –0.901
CCDC	2032982	2032974	2032973

$R_{int} = \sum |F_o^2 - F_{o,mean}^2| / \sum F_o^2$, $S = [\sum(w(F_o^2 - F_c^2)^2)/(N_{diffrs} - N_{params})]^{½}$ for all data, $R(F) = \sum ||F_o| - |F_c|| / \sum |F_o|$ for observed data, $wR(F^2) = [\sum(w(F_o^2 - F_c^2)^2)/(\sum w(F_o^2)^2)]^{½}$ for all data.

Table S1 (continuation). Crystal data and structure refinement of studied compounds.

	5	**6**	**7**
Formula	$C_{12}H_{12}ClGeN_3$	$C_{20}H_{16}GeN_6$	$C_{20}H_{16}N_6Sn$
Formula weight, g mol^{-1}	306.29	412.98	459.08
Crystal system	Monoclinic	Orthorhombic	Monoclinic
Crystal size, mm	0.59 × 0.39 × 0.38	0.37 × 0.29 × 0.22	0.59 × 0.57 × 0.16
Space group	$P2_1/c$	Pbca	$P2_1/n$
a, Å	7.9626(5)	7.7879(4)	11.8487(6)
b, Å	9.3447(5)	18.4219(11)	9.2747(4)
c, Å	17.4878(10)	24.4619(12)	16.9821(9)
α, º	90	90	90
β, º	95.358(2)	90	104.129(2)
γ, º	90	90	90
V, Å^3	1295.55(13)	3509.5(3)	1809.76(15)
Z	4	8	4
ρ_{calcd}, Mg m^{-3}	1.570	1.563	2.022
μ (Mo $K\alpha$), mm^{-1}	2.551	1.764	1.429
F(000)	616	1680	912
θ range, deg	1 to 27.5	1 to 27.5	1 to 27.5
No. of reflns collected	33637	31981	38955
No. indep. Reflns	2972	4018	4154
No. obsd reflns with ($I>2\sigma(I)$), R_{int}	2561, 0.0296	2848, 0.058	3733, 0.017
No. refined params	156	244	244
GooF (F^2)	1.086	1.057	1.147
R_1 (F) ($I > 2\sigma(I)$)	0.0301	0.0473	0.0226
wR_2 (F^2) (all data)	0.0607	0.0740	0.0530
Largest diff peak/hole, e Å^{-3}	0.377 / –0.372	0.392 / –0.489	0.370 / –0.651
CCDC	2032978	2032972	2032975

$R_{int} = \sum |F_o^2 - F_{o,mean}^2| / \sum F_o^2$, $S = [\sum(w(F_o^2 - F_c^2)^2)/(N_{diffrs} - N_{params})]^{½}$ for all data, $R(F) = \sum ||F_o| - |F_c|| / \sum |F_o|$ for observed data, $wR(F^2) = [\sum(w(F_o^2 - F_c^2)^2)/(\sum w(F_o^2)^2)]^{½}$ for all data.

Table S1 (continuation). Crystal data and structure refinement of studied compounds.

	8	**9**	**10**
Formula	$C_{24}H_{24}GeN_6$	$C_{24}H_{24}N_6Sn$	$C_{36}H_{36}GeLiN_9$
Formula weight, g mol^{-1}	469.08	515.18	674.27
Crystal system	Triclinic	Monoclinic	trigonal
Crystal size, mm	0.59 × 0.57 × 0.23	0.59 × 0.34 × 0.28	0.59 × 0.59 × 0.48
Space group	P-1	$P2_1/c$	R3c
a, Å	8.8339(5)	11.4993(5)	12.0085(9)
b, Å	12.1659(6)	21.1590(8)	12.0085(9)
c, Å	12.3964(6)	9.1723(4)	41.775(3)
α, º	111.554(2)	90	90
β, º	96.379(2)	92.591(2)	90
γ, º	110.358(2)	90	120
V, Å^3	1117.25(10)	2229.46(16)	5217.0(9)
Z	2	4	6
ρ_{calcd}, Mg m^{-3}	1.394	1.535	1.288
μ (Mo $K\alpha$), mm^{-1}	1.394	1.170	0.920
F(000)	484	1040	2100
θ range, deg	1 to 27.5	1 to 27.5	1 to 27.5
No. of reflns collected	36087	51074	18638
No. indep. Reflns	5147	5118	3418
No. obsd reflns with ($I>2\sigma(I)$), R_{int}	4703, 0.024	4672, 0.016	2917, 0.036
No. refined params	284	284	146
GooF (F^2)	1.035	1.138	1.039
R_1 (F) ($I > 2\sigma(I)$)	0.0258	0.0225	0.0312
wR_2 (F^2) (all data)	0.0644	0.0519	0.0626
Largest diff peak/hole, e Å^{-3}	0.272 / –0.459	0.298 / –0.613	0.208 / –0.279
CCDC	2032977	2032981	2032979

$R_{int} = \sum |F_o^2 - F_{o,mean}^2| / \sum F_o^2$, $S = [\sum(w(F_o^2 - F_c^2)^2)/(N_{diffrs} - N_{params})]^{½}$ for all data, $R(F) = \sum ||F_o| - |F_c|| / \sum |F_o|$ for observed data, $wR(F^2) = [\sum(w(F_o^2 - F_c^2)^2)/(\sum w(F_o^2)^2)]^{½}$ for all data.

Table S1 (continuation). Crystal data and structure refinement of studied compounds.

	11	**12**
Formula	$C_{36}H_{36}LiN_9Sn$	$C_{36}H_{36}LiN_9Pb$
Formula weight, g mol^{-1}	720.37	808.87
Crystal system	trigonal	trigonal
Crystal size, mm	0.59 × 0.52 × 0.42	0.24 × 0.23 × 0.18
Space group	R3c	R3c
a, Å	12.1177(4)	19.4667(12)
b, Å	12.1177(4)	19.4667(12)
c, Å	41.8064(14)	15.6860(12)
α, º	90	90
β, º	90	90
γ, º	120	120
V, Å^3	5316.4(12)	5147.9(7)
Z	6	6
ρ_{calcd}, Mg m^{-3}	1.350	1.565
μ (Mo $K\alpha$), mm^{-1}	0.759	4.955
F(000)	2208	2400
θ range, deg	1 to 27.5	1 to 27.5
No. of reflns collected	11757	20507
No. indep. Reflns	2922	2619
No. obsd reflns with ($I>2\sigma(I)$), R_{int}	2405, 0.040	2295, 0.048
No. refined params	146	144
GooF (F^2)	1.098	1.061
R_1 (F) ($I > 2\sigma(I)$)	0.0288	0.0352
wR_2 (F^2) (all data)	0.0592	0.0793
Largest diff peak/hole, e Å^{-3}	0.665 / –0.377	1.899 / –1.527
CCDC	2032976	2032980

$R_{int} = \sum |F_o^2 - F_{o,mean}^2| / \sum F_o^2$, $S = [\sum(w(F_o^2 - F_c^2)^2)/(N_{diffrs} - N_{params})]^{½}$ for all data, $R(F) = \sum ||F_o| - |F_c|| / \sum |F_o|$ for observed data, $wR(F^2) = [\sum(w(F_o^2 - F_c^2)^2)/(\sum w(F_o^2)^2)]^{½}$ for all data.

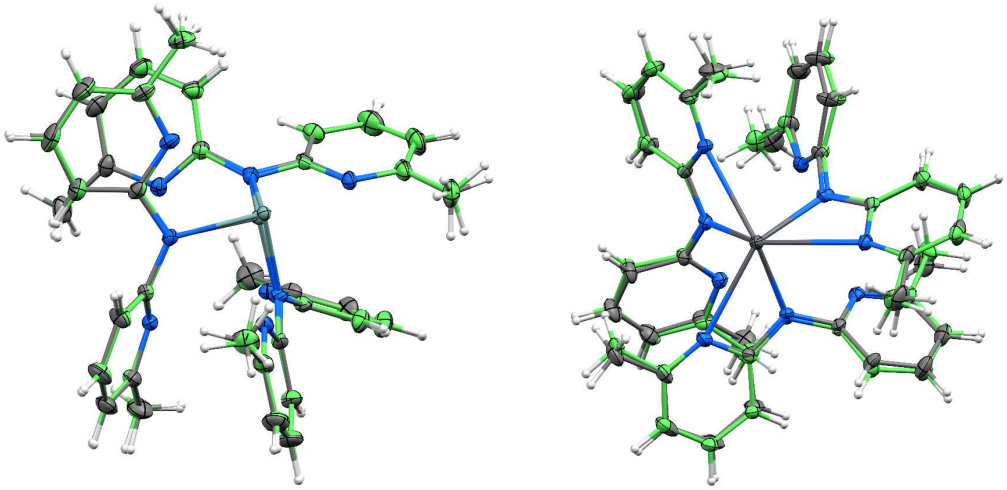

Figure S39: Overlay complexes structures of **10**-**12**: Sn (grey) and Ge (green) (left); Sn (grey) and Pb (green) (right). Li atoms were removed.

3. Theoretical study

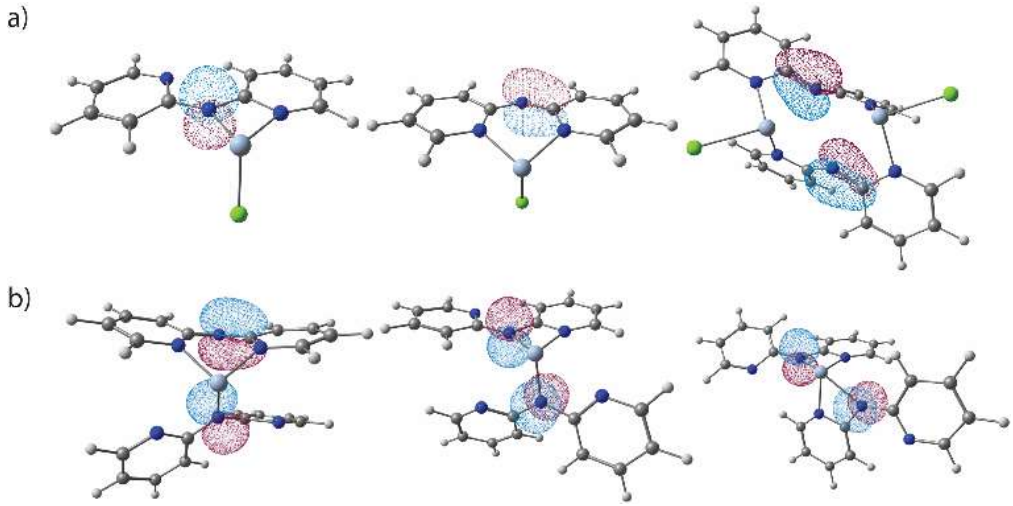

Figure S40: p-orbital associated with bridging nitrogen of *dpa* ligand in different coordination modes for heteroleptic chlorogermylenes (a) and homoleptic $(dpa)_2Ge$ compounds (b).

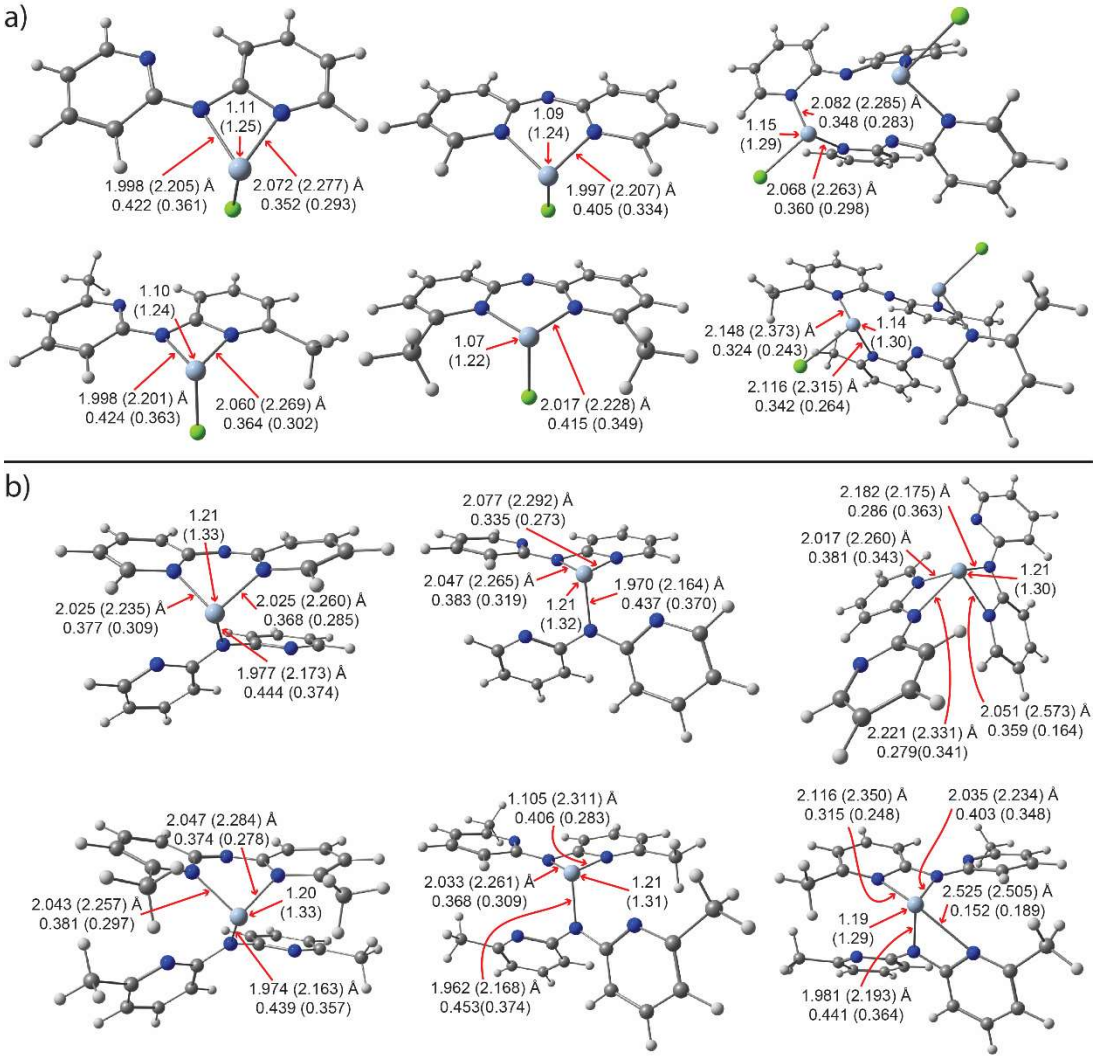

Figure S41: Calculated bond lengths, Wiberg bond indicies and natural charges for *dpa*- and *Me-dpa* Ge and Sn (in bracket) compounds.

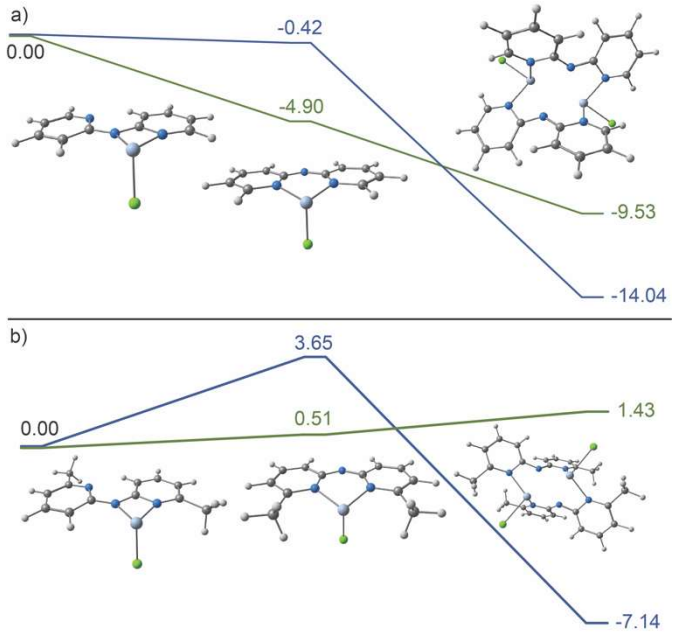

Figure S42: Relative energies between optimized structures (M062X/def2-TZVP level of theory) of chlorogermylenes (green curve) and chlorostannylenes (blue curve) with different arrangement of *dpa* (a) and Me-*dpa* (b) ligand. Electronic energies, given in kcal/mol are related to respective species with four-membered *N,N*-chelate ring.

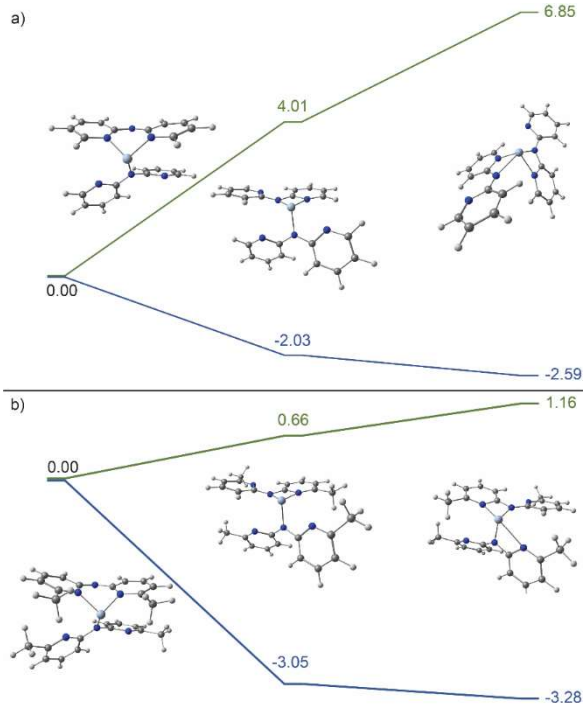

Figure S43: Relative energies between optimized structures (M062X/def2-TZVP level of theory) of homoleptic Ge (green curves) and Sn (blue curves) complexes with different arrangement of *dpa* (a) and *Me-dpa* (b) ligand respectively. Electronic energies, given in kcal/mol are related to respective species with six-membered *N,N*-chelate ring.

Table S2. Topological properties of BCPs for complexes **10-11a** in a.u.[a]

Complex	Bond	$\rho(r_{cp})$	$\nabla^2\rho(r_{cp})$	$G(r_{cp})$	$V(r_{cp})$	$H(r_{cp})$
10	Li4…N(5, 32, 59)	0.023 0.023 0.023	0.017 0.017 0.017	0.034 0.034 0.034	-0.025 -0.025 -0.025	0.009 0.009 0.009
10a	Ge119…Li3	0.018	0.081	0.017	-0.014	0.003
11	Li3…N(4, 31, 58)	0.022 0.022 0.022	0.162 0.162 0.162	0.032 0.032 0.032	-0.023 -0.023 -0.023	0.009 0.009 0.009
11a	Sn1…Li4	0.016	0.061	0.013	-0.011	0.002

[a]$\rho(r_{cp})$ - the electron density, $\nabla^2\rho(r_{cp})$ - the Laplacian function of the electron density, $G(r_{cp})$ - the kinetic electron energy density, $V(r_{cp})$ - the potential electron energy density, $H(r_{cp})$ - the total electron energy density.

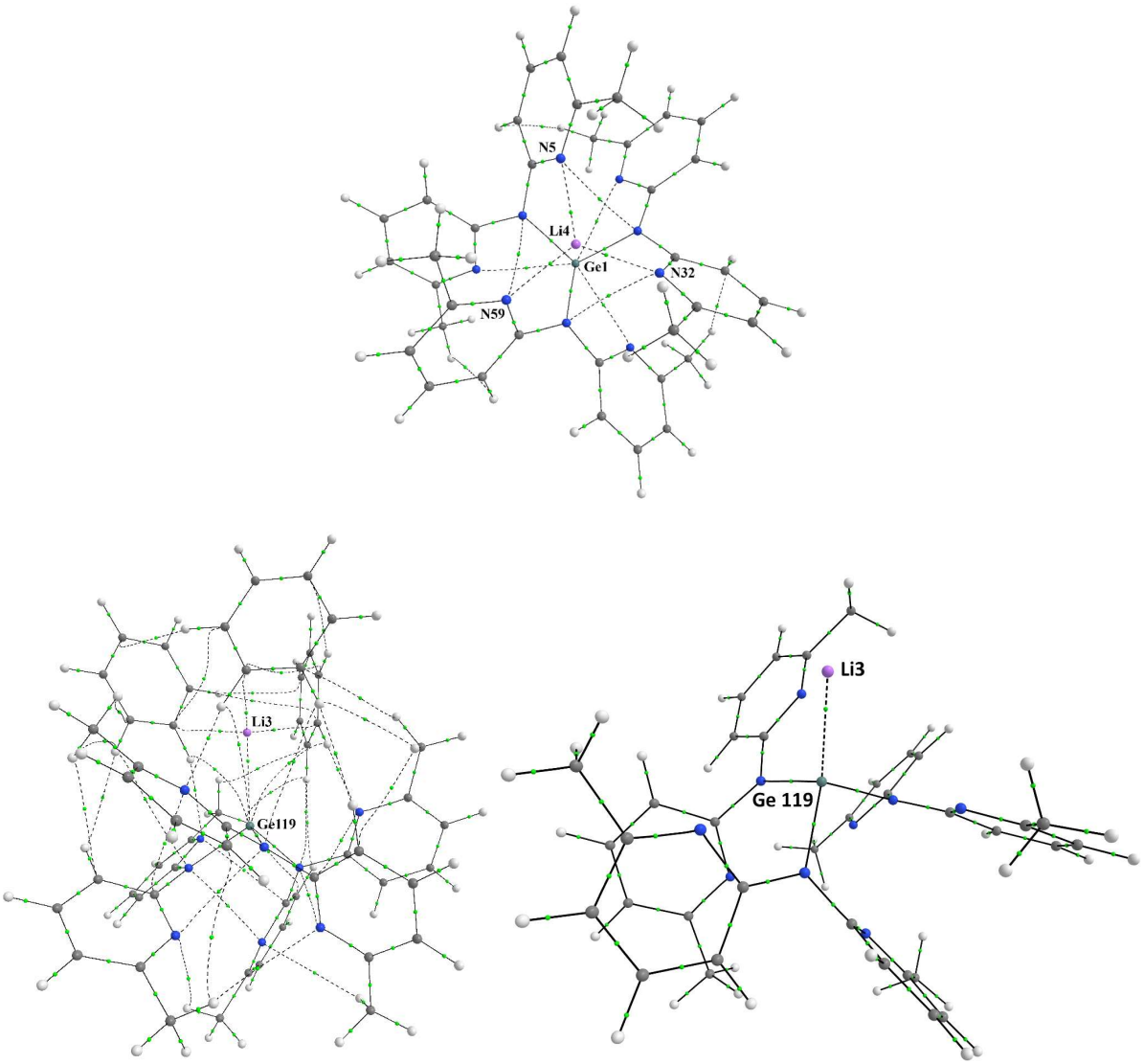

Figure S44: Molecular graphs of complexes **10** and **10a** / the key fragment of it. Only critical points (3, -1) are presented for clarity (green).

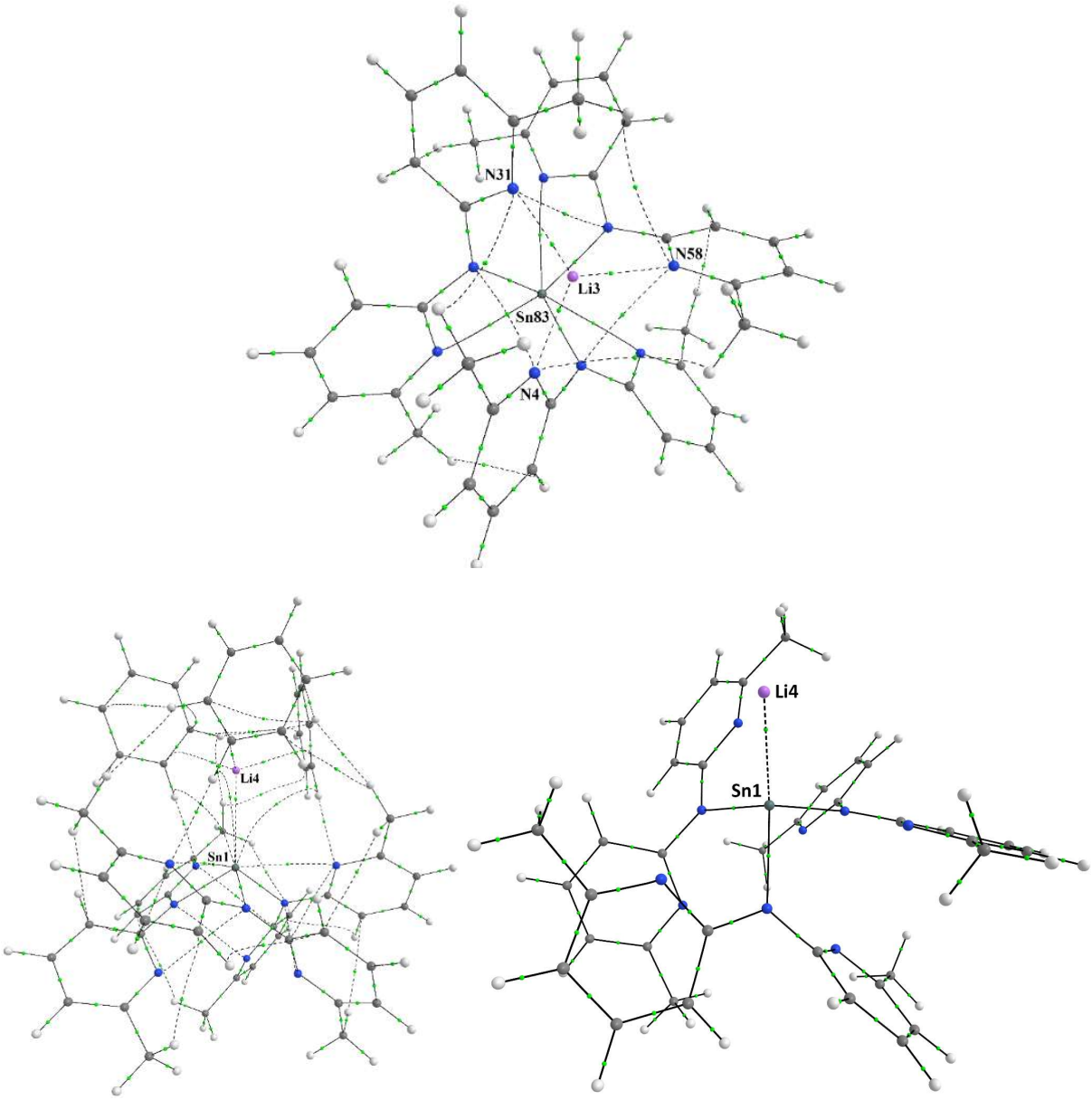

Figure S45: Molecular graphs of complexes **11** and **11a** / the key fragment of it. Only critical points (3, -1) are presented for clarity (green).

Table S3: Energy values of HOMO and LUMO in eV.

Complex			
	10	**11**	**12**
HOMO	-4.77	-5.01	-5.21
LUMO	-0.73	-0.66	-0.61
HOMO-2			-5.24
Complex			
	10a	**11a**	**12a**
HOMO	-4.70	-4.76	-4.77
LUMO	-0.99	-1.14	-1.41
HOMO-3			-5.78

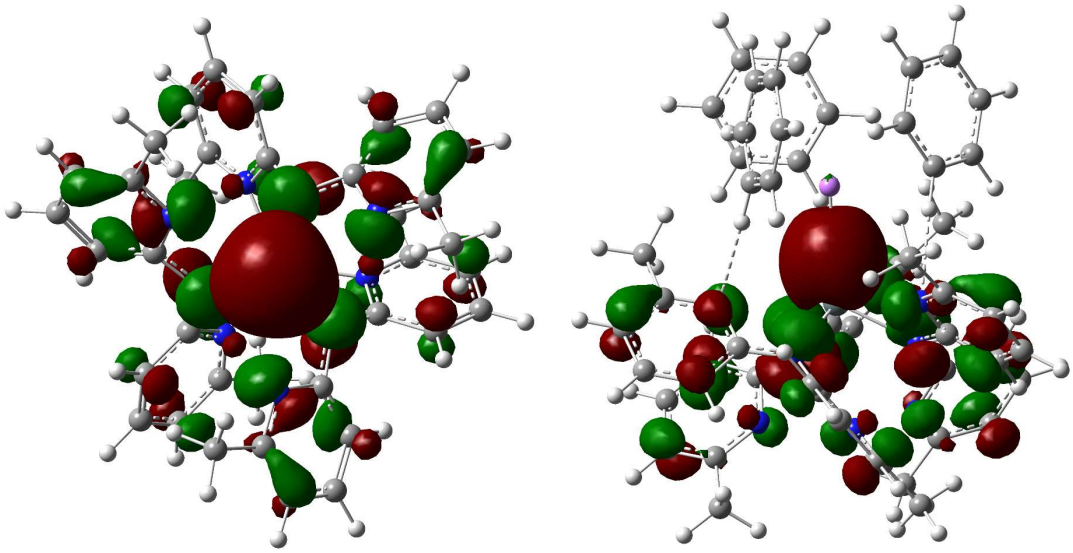

Figure S46: The HOMO orbitals for **11** and **11a** complexes (isovalue = 0.03).

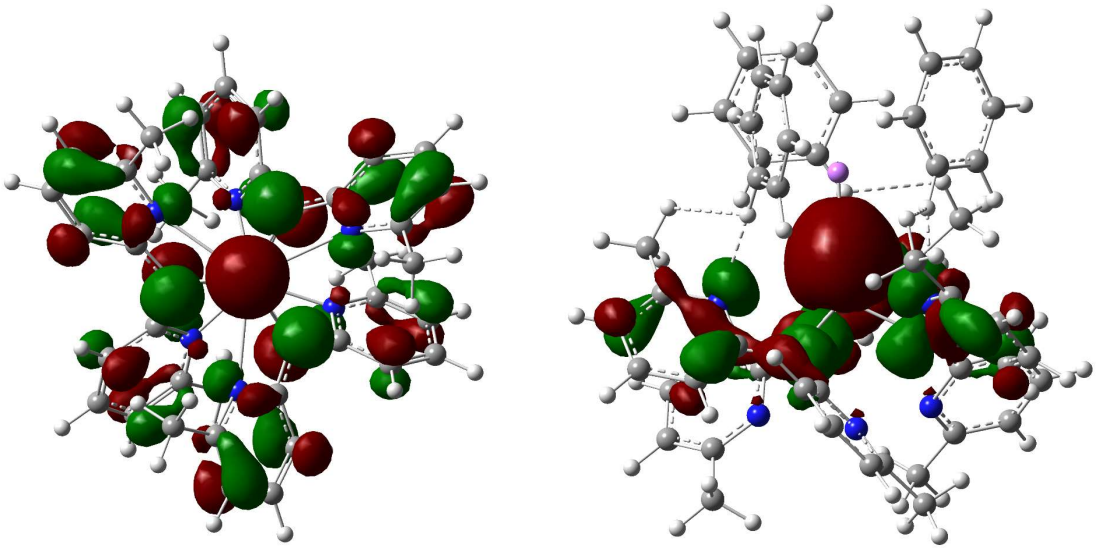

Figure S47: The HOMO-2 orbital for **12** and HOMO-3 for **12a** complexes (isovalue = 0.03).